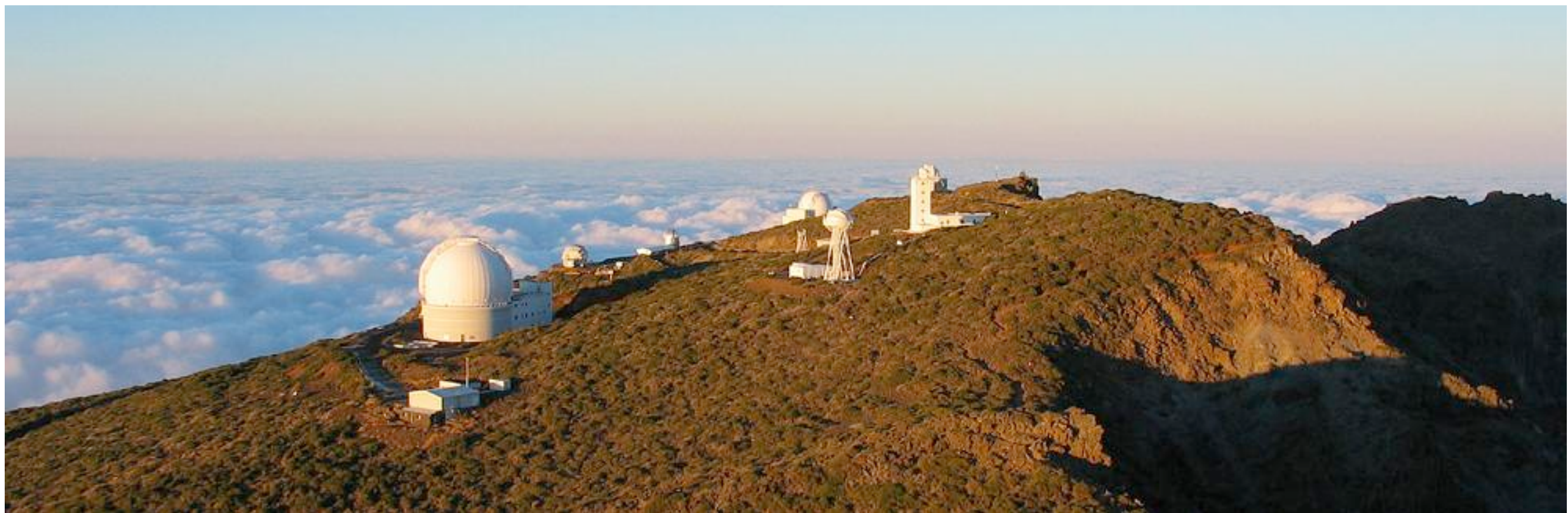
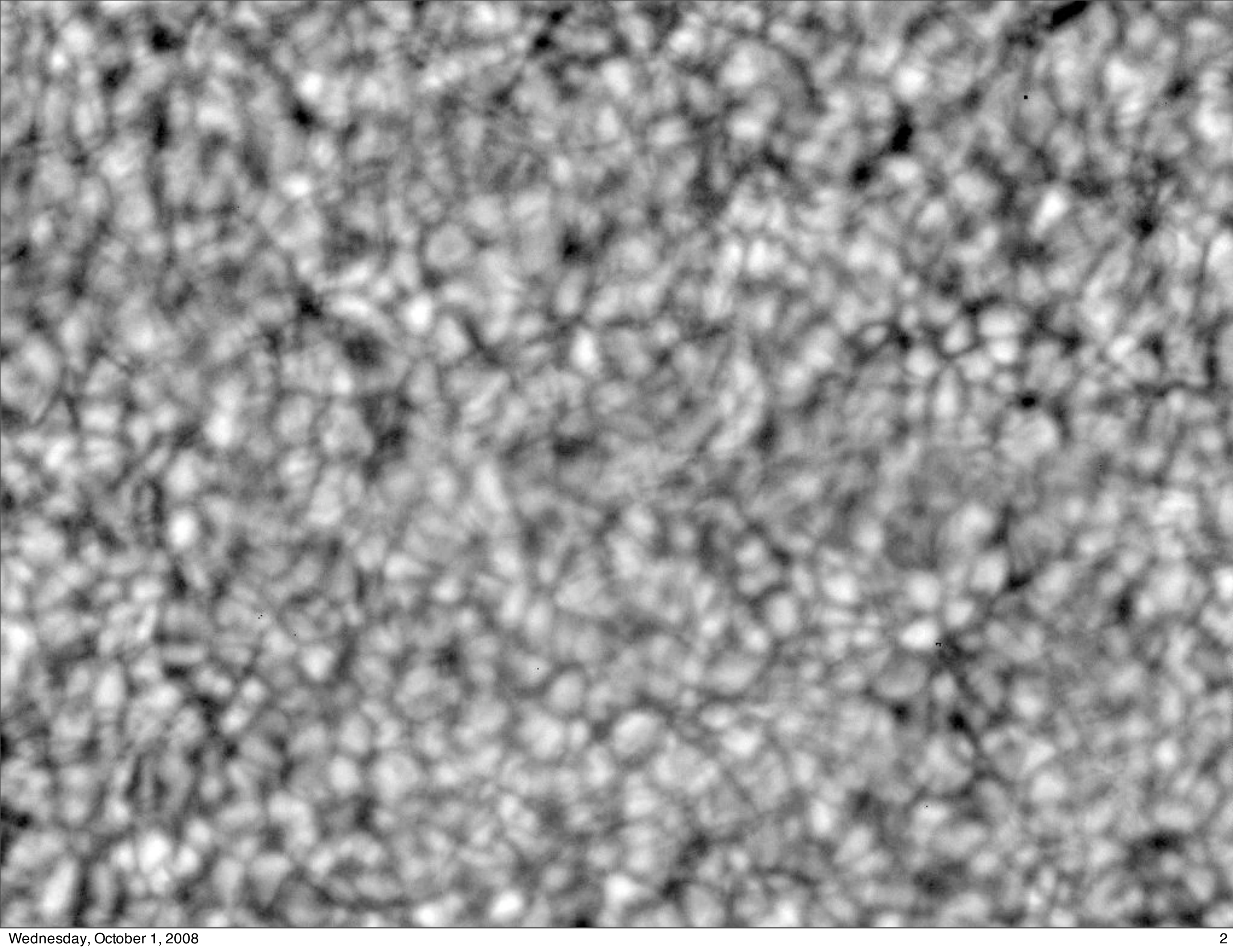


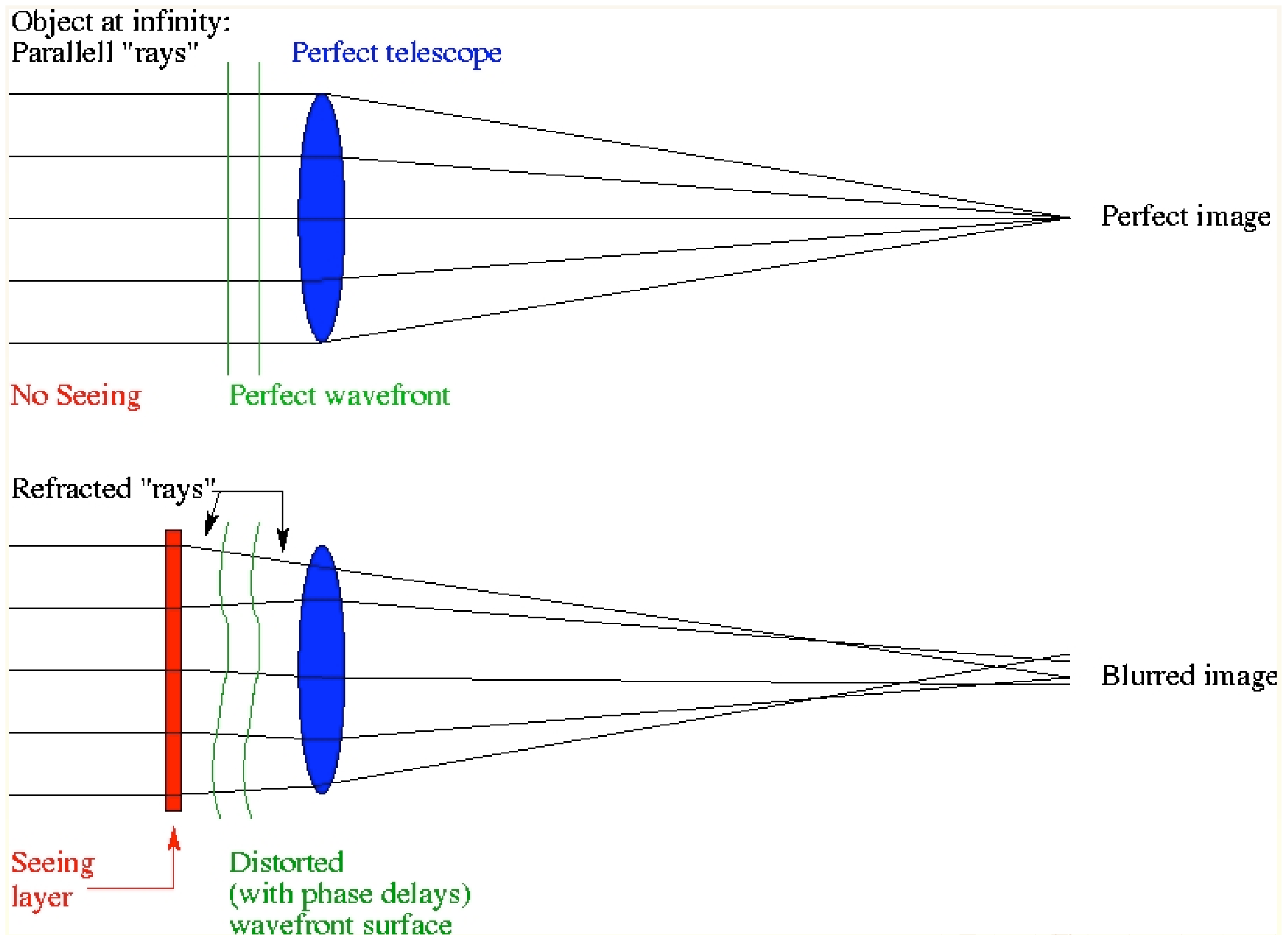
high-resolution imaging techniques

Luc Rouppe van der Voort



ITA lecture, October 1, 2008





origin of seeing

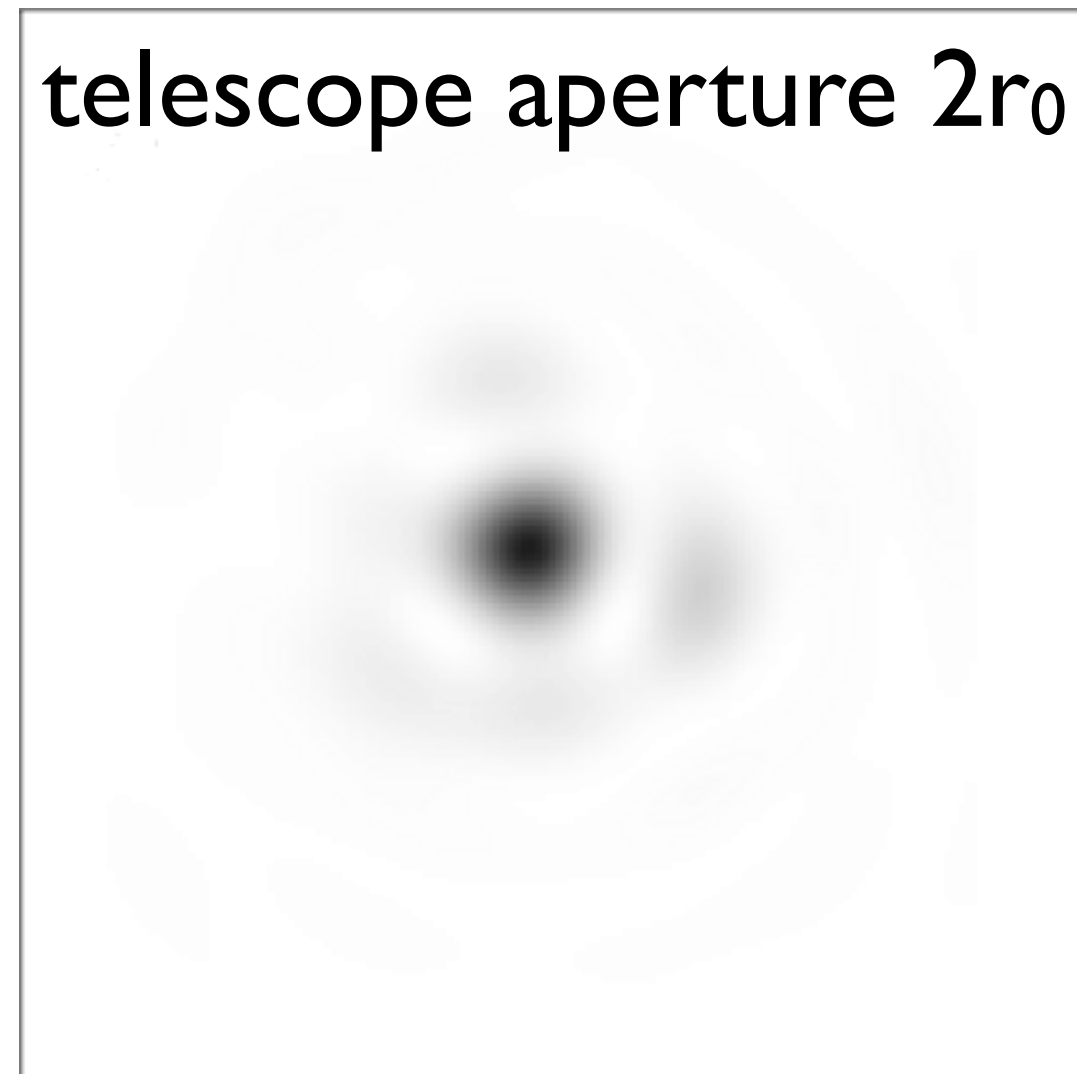
- Temperature fluctuations in air cause fluctuations in refractive index.
- Variations in refractive index cause refraction of rays = wavefront phase delays.
- Seeing statistics usually follows Kolmogorov statistics.

seeing parameters r_0 , t_0

- time scale t_0 over which turbulence becomes significant
- length scale r_0 over which turbulence becomes significant: Fried parameter

Fried parameter r_0

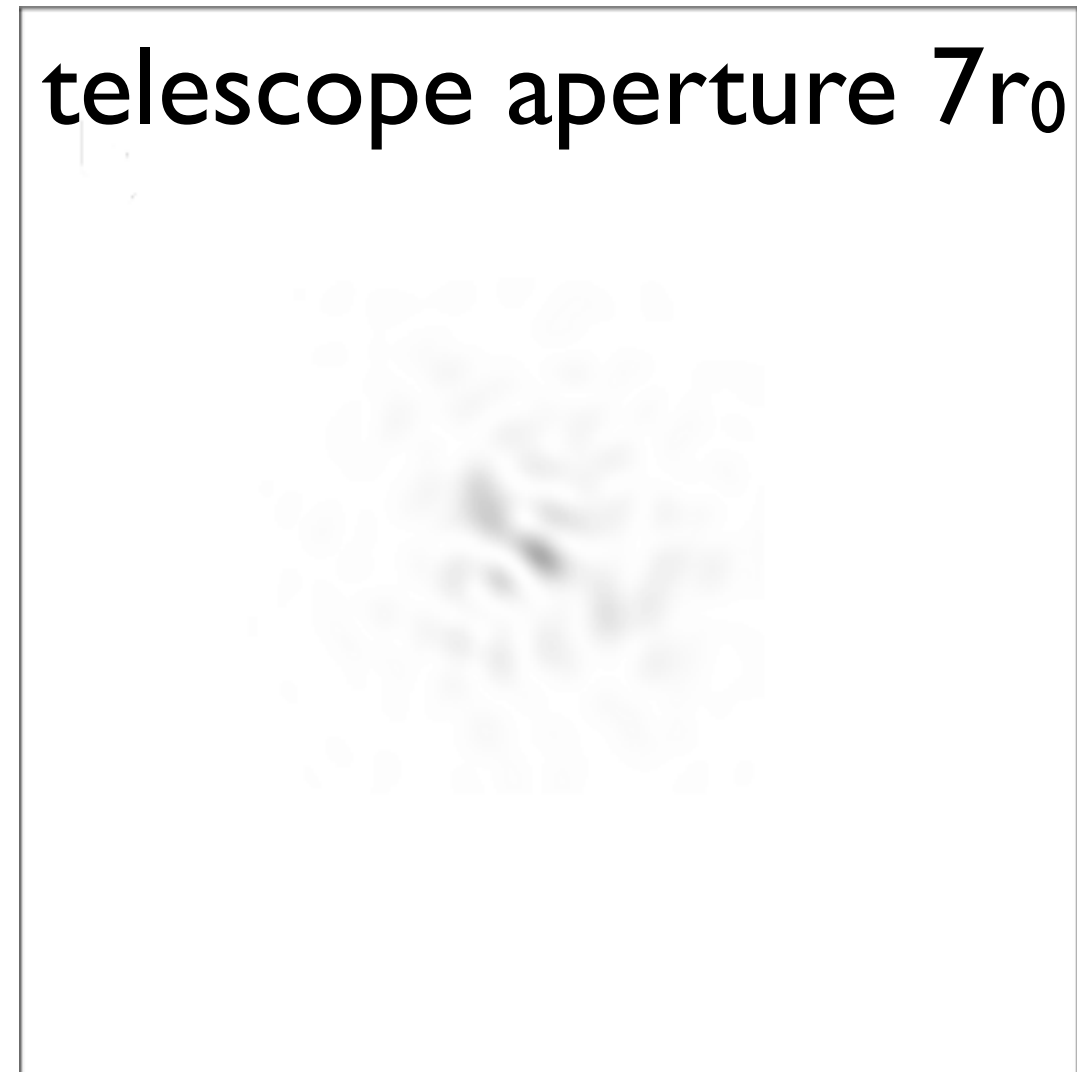
telescope aperture $2r_0$



simulated negative image of point source (star)

Fried parameter r_0

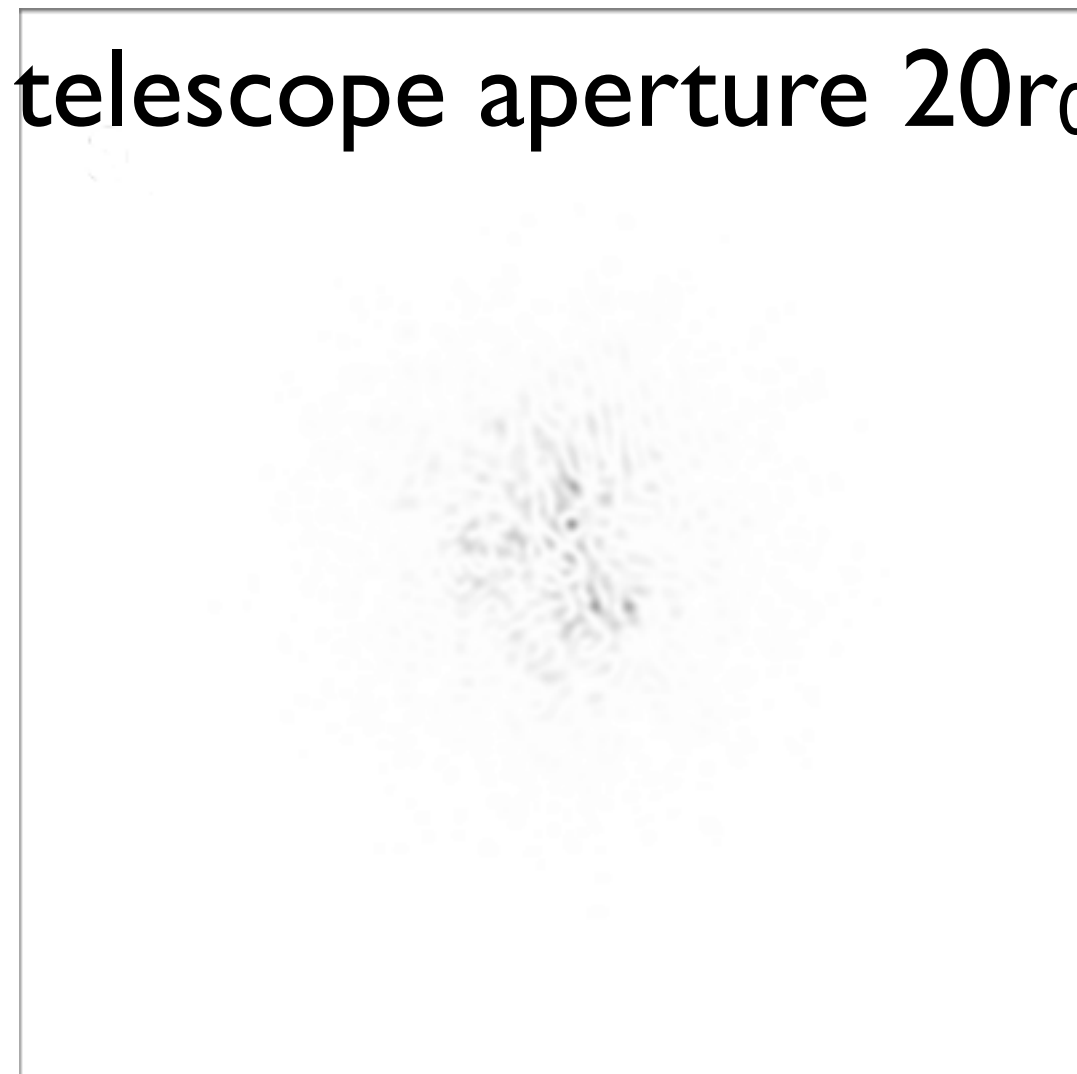
telescope aperture $7r_0$



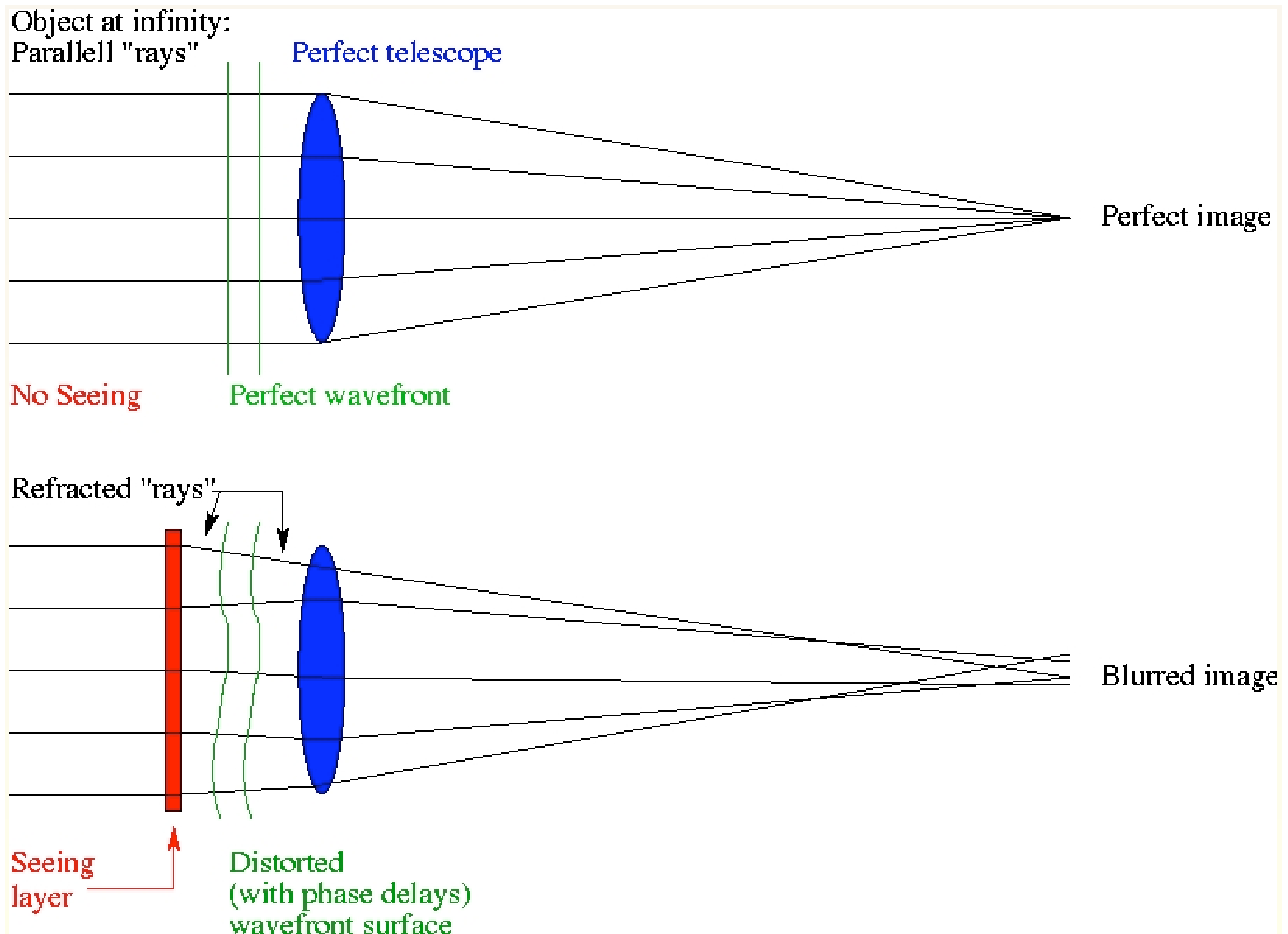
simulated negative image of point source (star)

Fried parameter r_0

telescope aperture $20r_0$

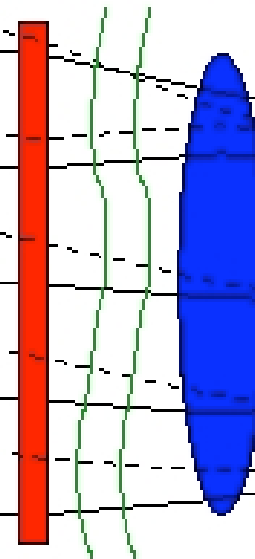


simulated negative image of point source (star)



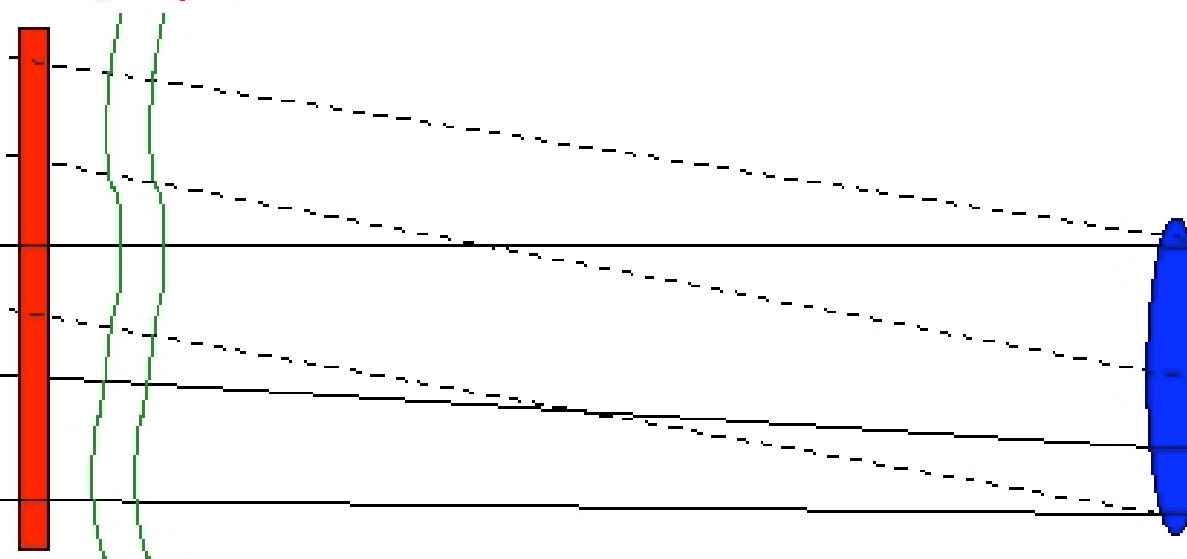
ANISOPLANATISM

Seeing layer



Local (near telescope) seeing: Point spread function the SAME across the field-of-view

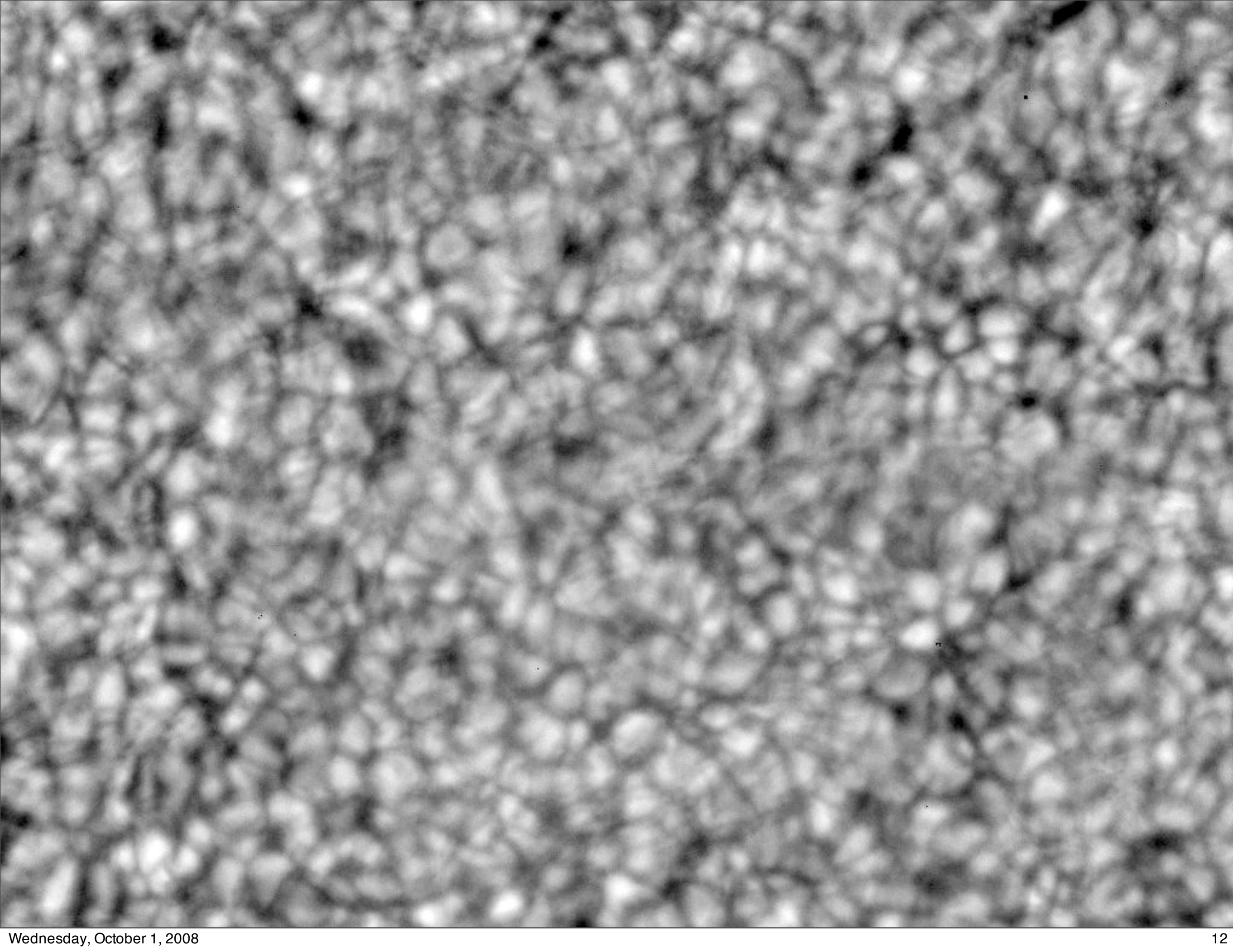
Seeing layer

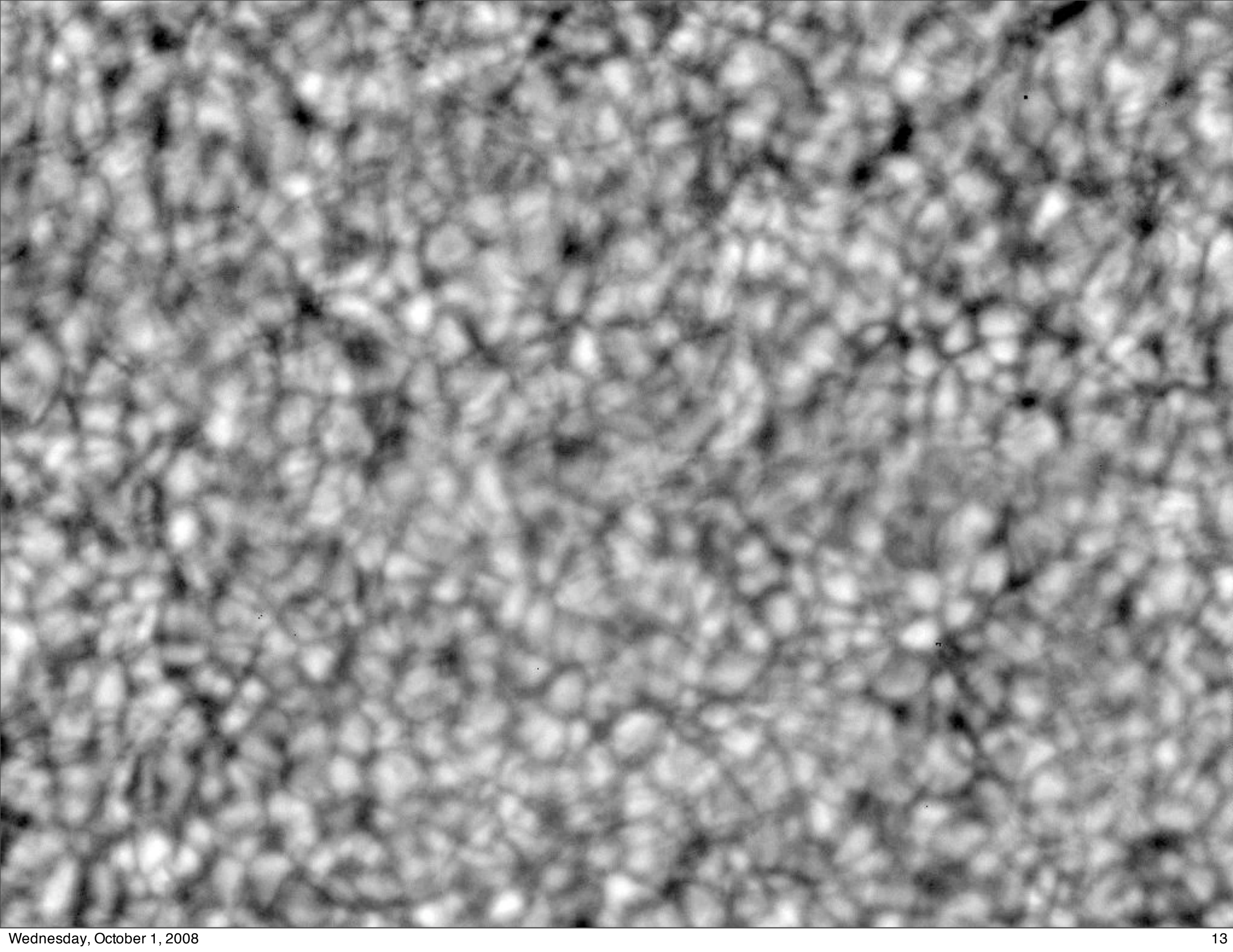


High-altitude seeing: Point-spread function VARIES across the field-of-view

anisoplanatism

- Seeing originating beyond a few hundred meters from the telescope causes variable seeing across field-of-view.
- High–altitude seeing (typically 10–20 km from the telescope) causes seeing variations over one or a few arcsec.
- isoplanatic angle θ_0 : $\theta_0 = 0.314 r_0 / h$, with h height of seeing layer
- $h=10 \text{ km}$, $r_0=15 \text{ cm}$ (good seeing): $\theta_0=1''$





Modal decomposition of wavefronts errors

Wavefront variations across the pupil can be expanded in a set of functions that are orthogonal over the telescope pupil.

$$W(\rho, \theta) = \sum c^m_n Z^m_n(\rho, \theta)$$

The diagram illustrates the components of the wavefront expansion equation. It features a central equation $W(\rho, \theta) = \sum c^m_n Z^m_n(\rho, \theta)$. Three arrows point from labels below the equation to its parts: one arrow points to $W(\rho, \theta)$ labeled "wavefront aberration", another points to c^m_n labeled "expansion coefficient", and a third points to $Z^m_n(\rho, \theta)$ labeled "Zernike polynomial".

Zernike polynomials

$Z^m_n(\rho, \theta) = N^m_n R^m_n \cos(m\theta)$ for $m \geq 0$, “even” functions
 $= -N^m_n R^m_n \sin(m\theta)$ for $m < 0$, “odd” functions

for given n : $m = -n, -n+2, -n+4, \dots, n$

with N^m_n normalization factor:

$N^m_n = [(2(n+1))/(1+\delta_m)]^{1/2}$ with $\delta_m = 1$ for $m=0$,
and $\delta_m = 0$ for $m \neq 0$

and radial polynomials R^m_n :

$$R_n^m(\rho) = \sum_{k=0}^{(n-m)/2} \frac{(-1)^k (n-k)!}{k! ((n+m)/2 - k)! ((n-m)/2 - k)!} \rho^{n-2k}$$

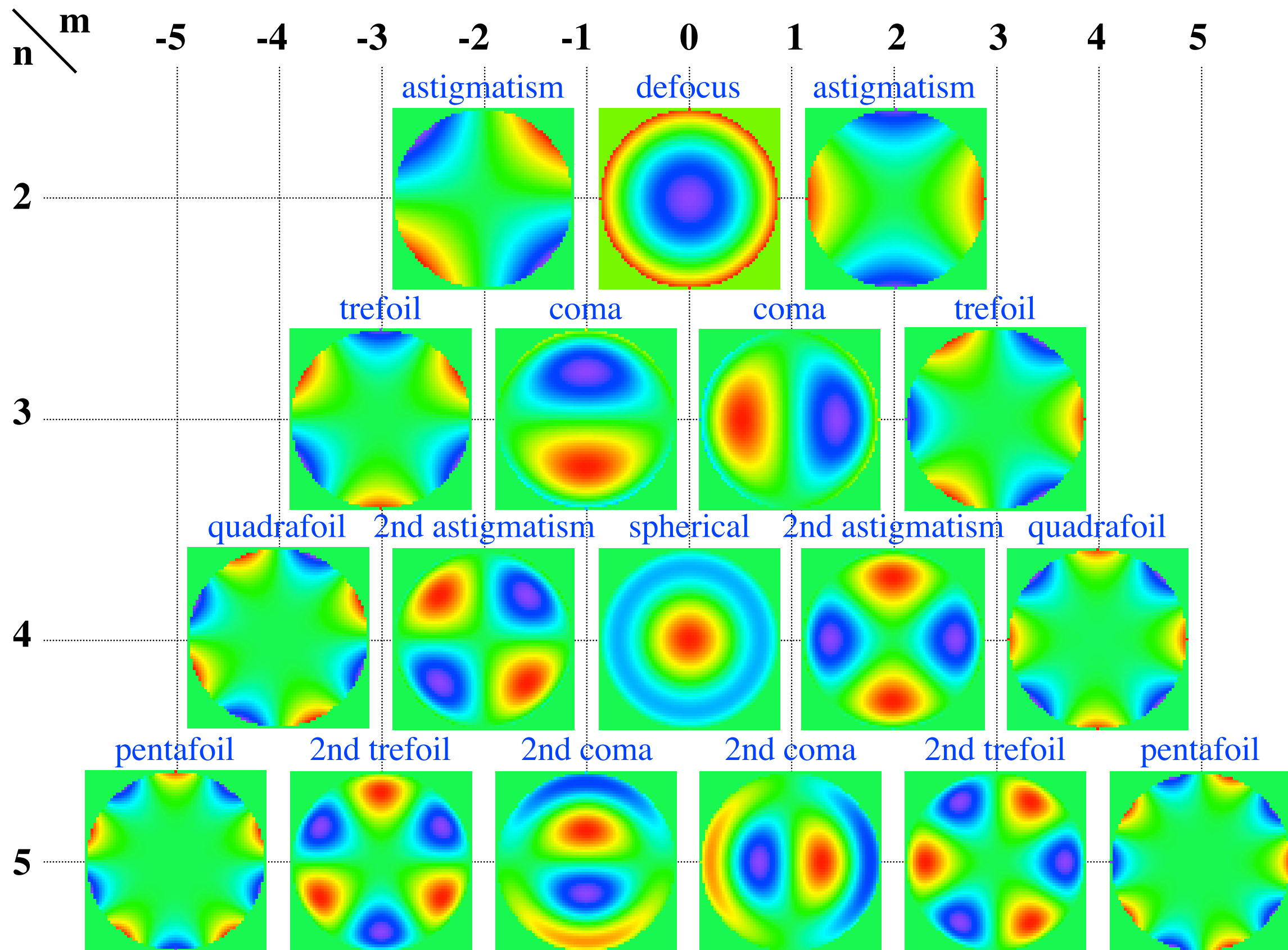
Zernike polynomials

$n =$ order	$m =$ frequency	$Z_n^m(\rho, \theta)$
0	0	1
1	-1	$2 \rho \sin \theta$
1	1	$2 \rho \cos \theta$
2	-2	$\sqrt{6} \rho^2 \sin 2\theta$
2	0	$\sqrt{3} (2\rho^2 - 1)$
2	2	$\sqrt{6} \rho^2 \cos 2\theta$
3	-3	$\sqrt{8} \rho^3 \sin 3\theta$
3	-1	$\sqrt{8} (3\rho^3 - 2\rho) \sin \theta$
3	1	$\sqrt{8} (3\rho^3 - 2\rho) \cos \theta$
3	3	$\sqrt{8} \rho^3 \cos 3\theta$
4	-4	$\sqrt{10} \rho^4 \sin 4\theta$
4	-2	$\sqrt{10} (4\rho^4 - 3\rho^2) \sin 2\theta$
4	0	$\sqrt{5} (6\rho^4 - 6\rho^2 + 1)$
4	2	$\sqrt{10} (4\rho^4 - 3\rho^2) \cos 2\theta$
4	4	$\sqrt{10} \rho^4 \cos 4\theta$
5	-5	$\sqrt{12} \rho^5 \sin 5\theta$
5	-3	$\sqrt{12} (5\rho^5 - 4\rho^3) \sin 3\theta$
5	-1	$\sqrt{12} (10\rho^5 - 12\rho^3 + 3\rho) \sin \theta$
5	1	$\sqrt{12} (10\rho^5 - 12\rho^3 + 3\rho) \cos \theta$
5	3	$\sqrt{12} (5\rho^5 - 4\rho^3) \cos 3\theta$

Second order
aberrations

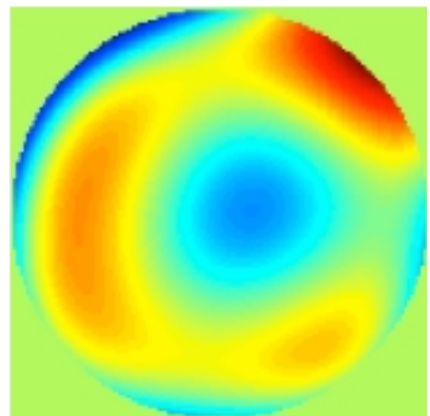
Higher order
aberrations

Wavefront mode for each Zernike polynomial



Wavefront aberration and Zernike expansion

$$W(\rho, \theta) = \sum c^m_n Z^m_n(\rho, \theta)$$



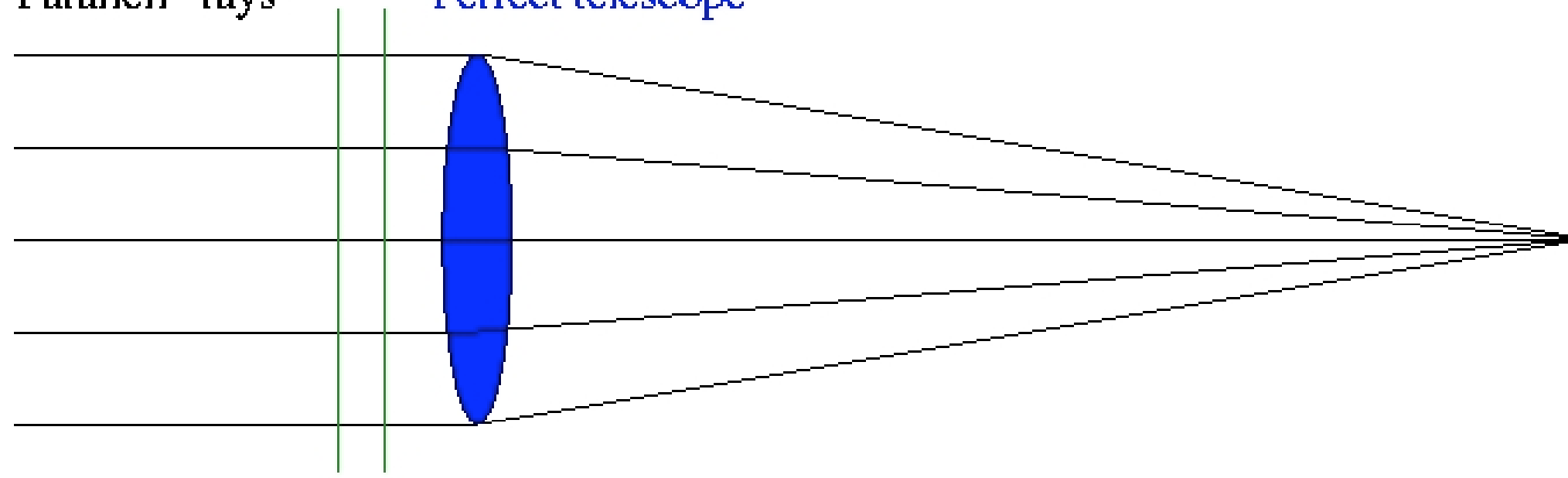
$$= -0.3 \begin{array}{c} \text{Circular heatmap} \\ \text{with a central peak} \end{array} + 0.5 \begin{array}{c} \text{Circular heatmap} \\ \text{with a central dip} \end{array} + 0.4 \begin{array}{c} \text{Circular heatmap} \\ \text{with a central peak} \end{array} +$$

$$0.6 \begin{array}{c} \text{Circular heatmap} \\ \text{with a central dip} \end{array} - 0.5 \begin{array}{c} \text{Circular heatmap} \\ \text{with two diagonal lobes} \end{array} + 0.2 \begin{array}{c} \text{Circular heatmap} \\ \text{with two diagonal lobes} \end{array} +$$

$$0.4 \begin{array}{c} \text{Circular heatmap} \\ \text{with four lobes} \end{array} + \dots$$

Object at infinity:
Parallel "rays"

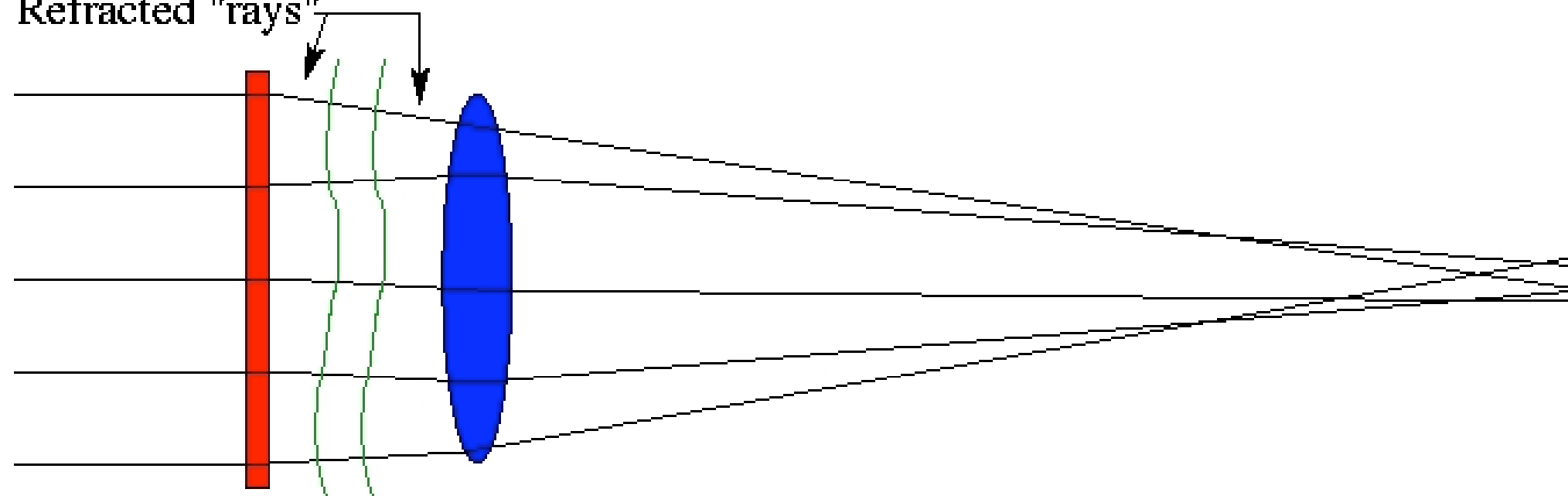
Perfect telescope



Perfect image

No Seeing Perfect wavefront

Refracted "rays"



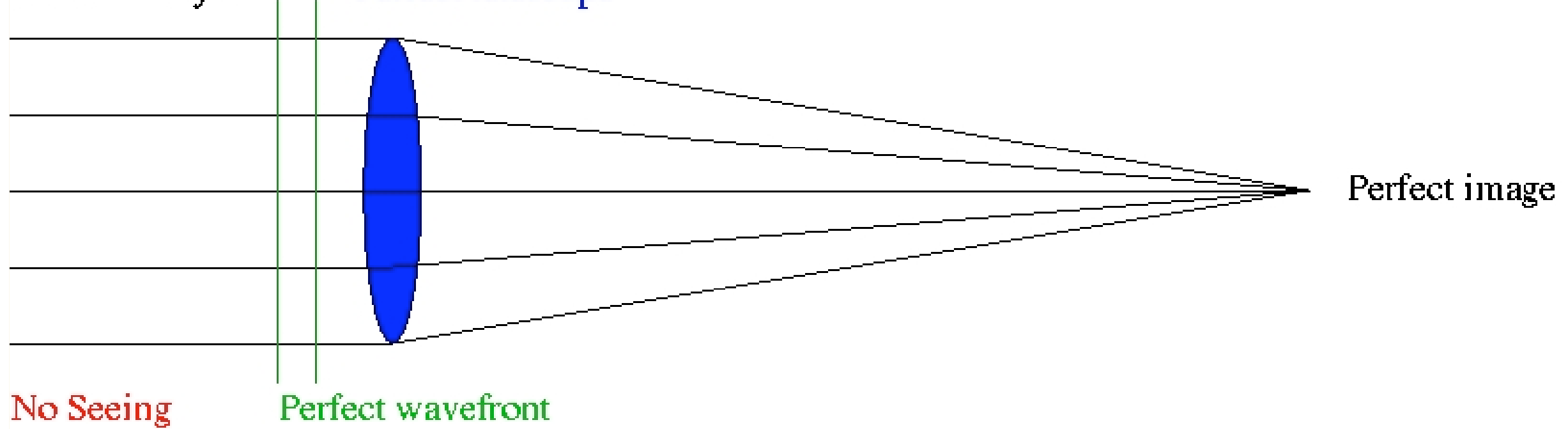
Blurred image

Seeing
layer

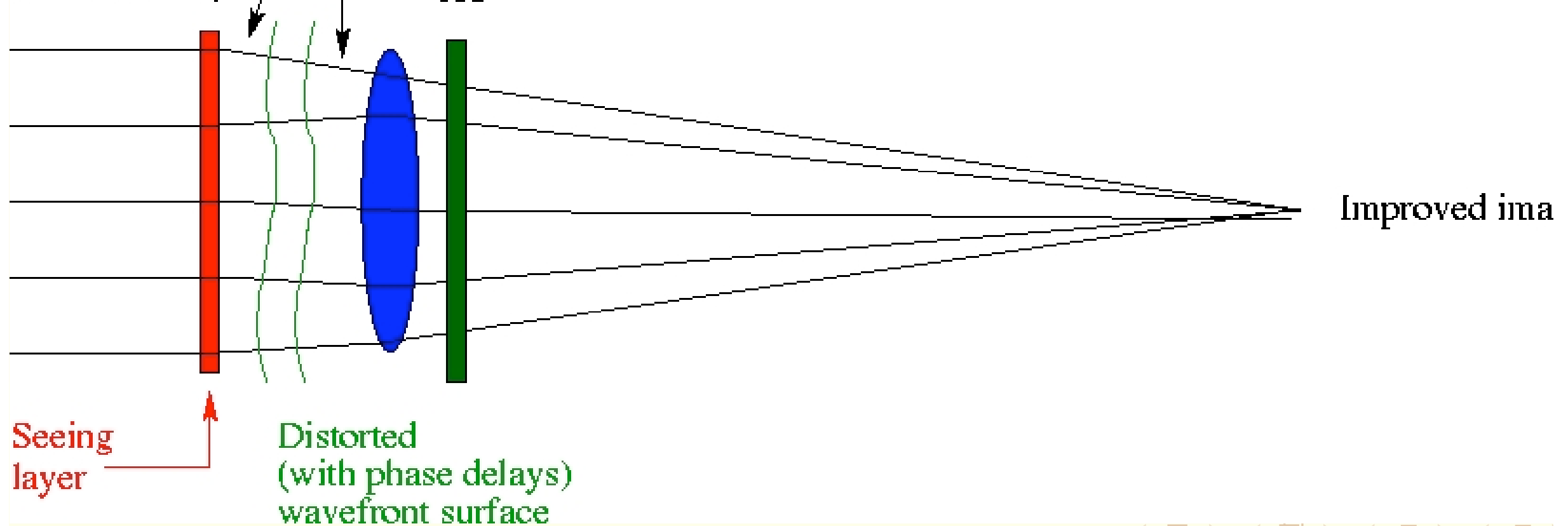
Distorted
(with phase delays)
wavefront surface

Object at infinity:
Parallel "rays"

Perfect telescope



Refracted "rays"
AO

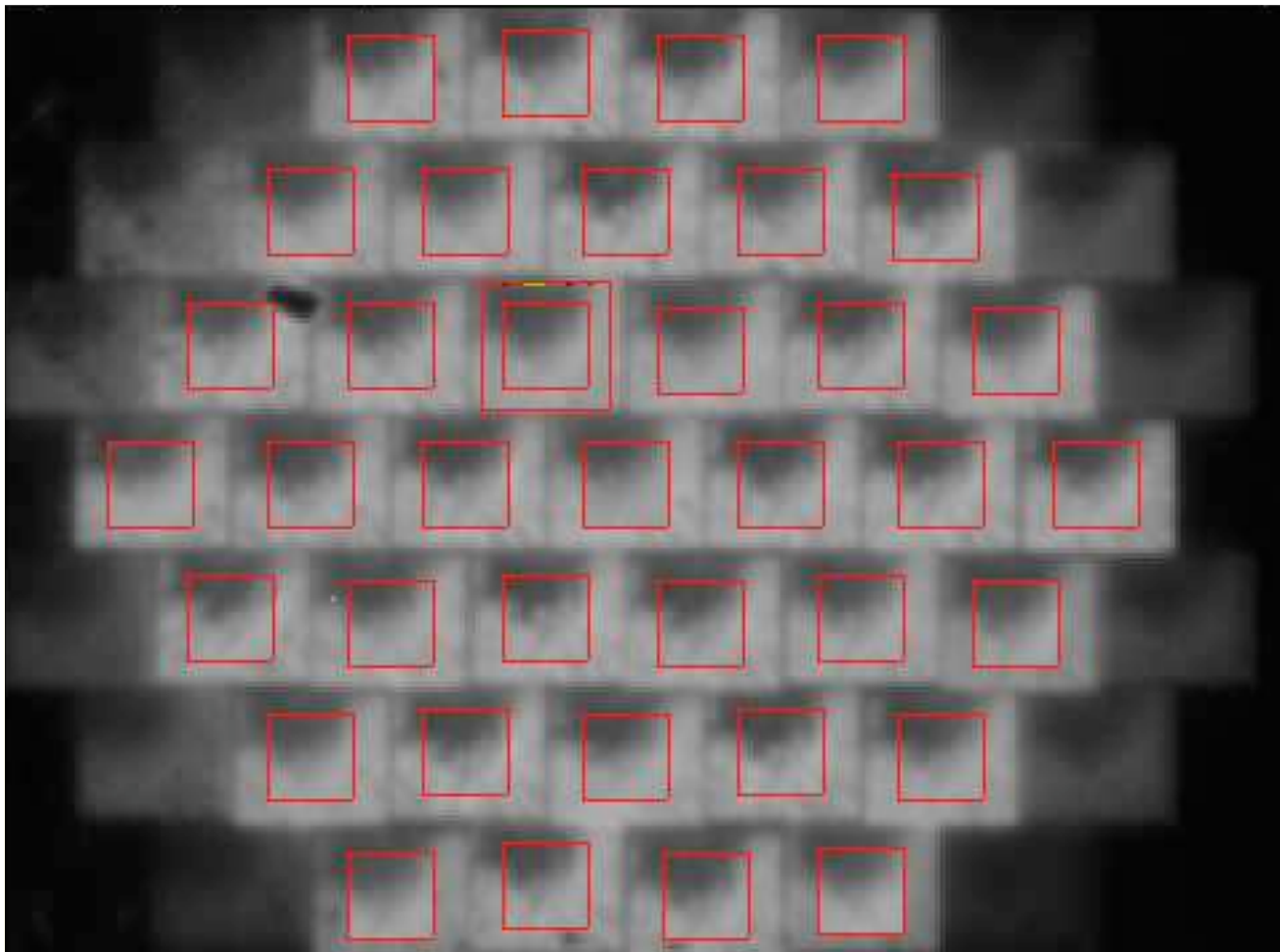


AO wavefront sensor

The most common wavefront sensor, the Shack–Hartmann wavefront sensor, is based on the following:

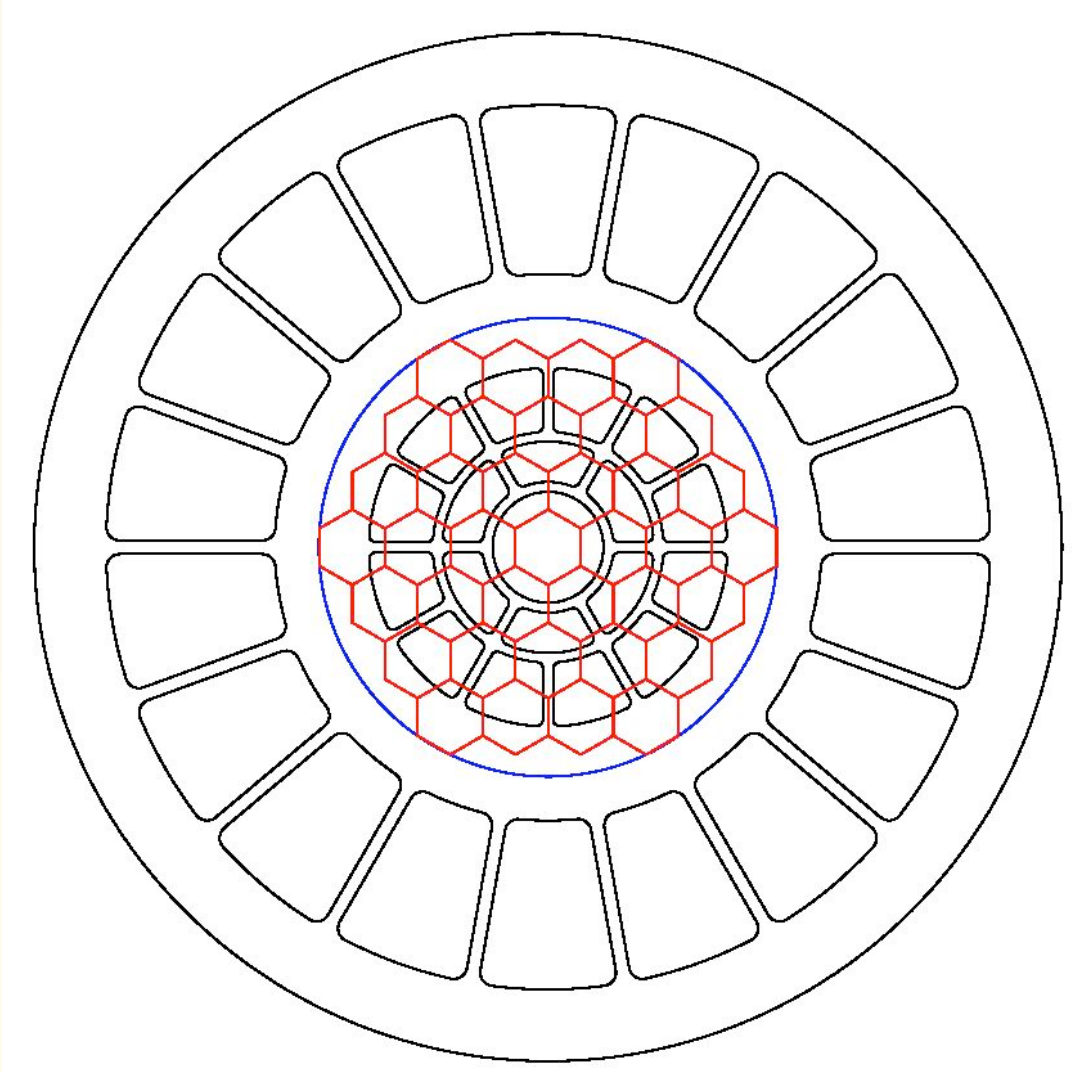
- Over the entire telescope pupil, the wavefront shows random variations including wavefront curvature, giving blurring of the image.
- Over small subsections of the aperture (diameter approximately equal to r_0 or less), the curvature terms are negligible, but wavefront tilt still significant. For such small subapertures, the corresponding subimages will be diffraction limited, but moving, as seeing changes. The movement of the sub-images directly measures the local slope (average gradient) of the wavefront over that subaperture.

the Shack-Hartmann wavefront sensor

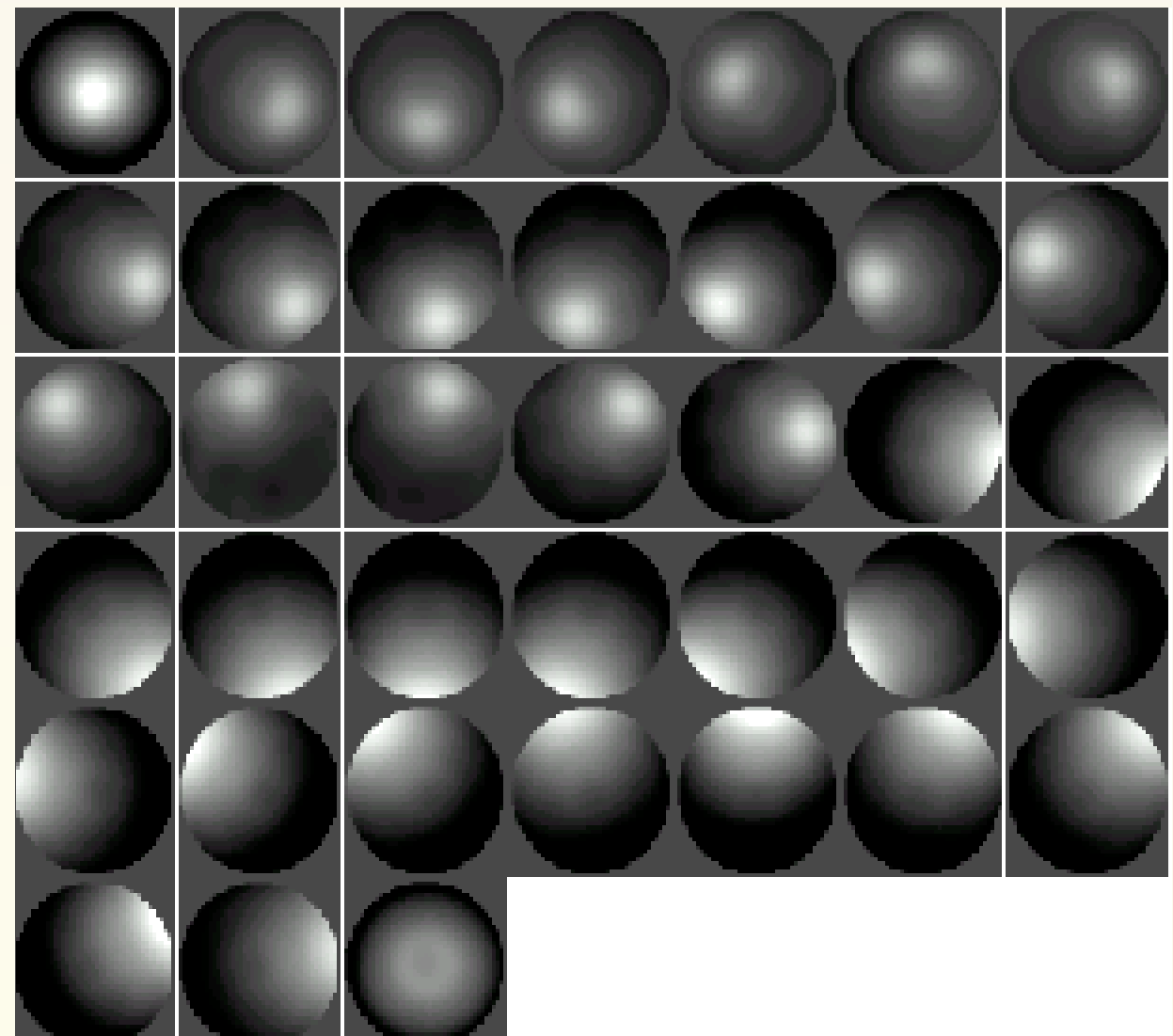


- Re-image telescope pupil on array of micro-lenses, with diameter equivalent to $\leq r_0$
- record sub-images with fast CCD camera
- measure x,y subimage movement to obtain mean wavefront gradient over each microlens
- Fit the measured wavefront gradients to a global (over the entire pupil) wavefront, using modal decomposition

SST AO system: 37-electrode bimorph deformable mirror



Mirror electrode geometry



Electrode responses

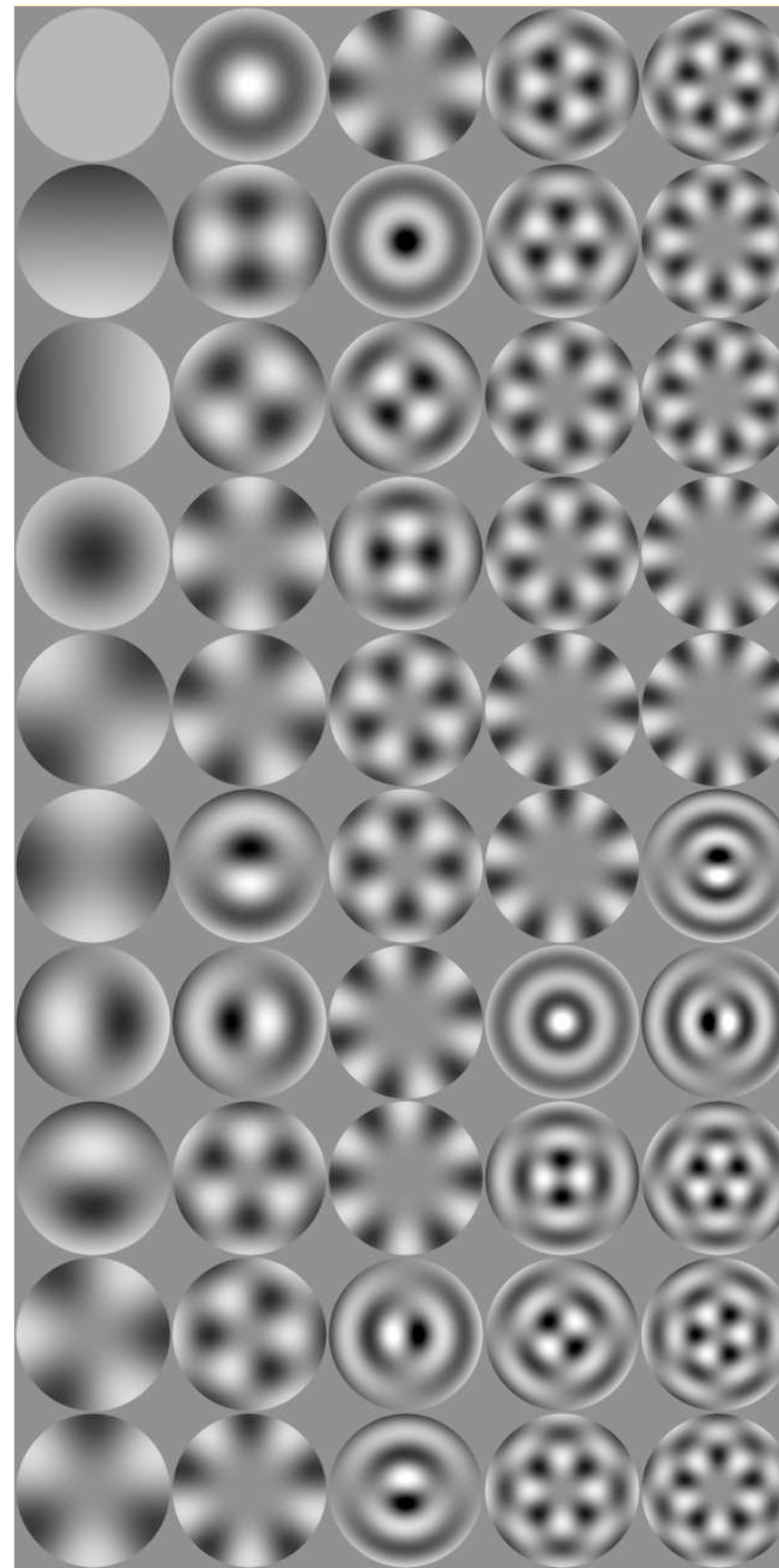
By controlling the adaptive mirror we can therefore compensate the atmospheric seeing effects by locally tilting the adaptive mirror surface such all sub-images remain in pre-determined positions.

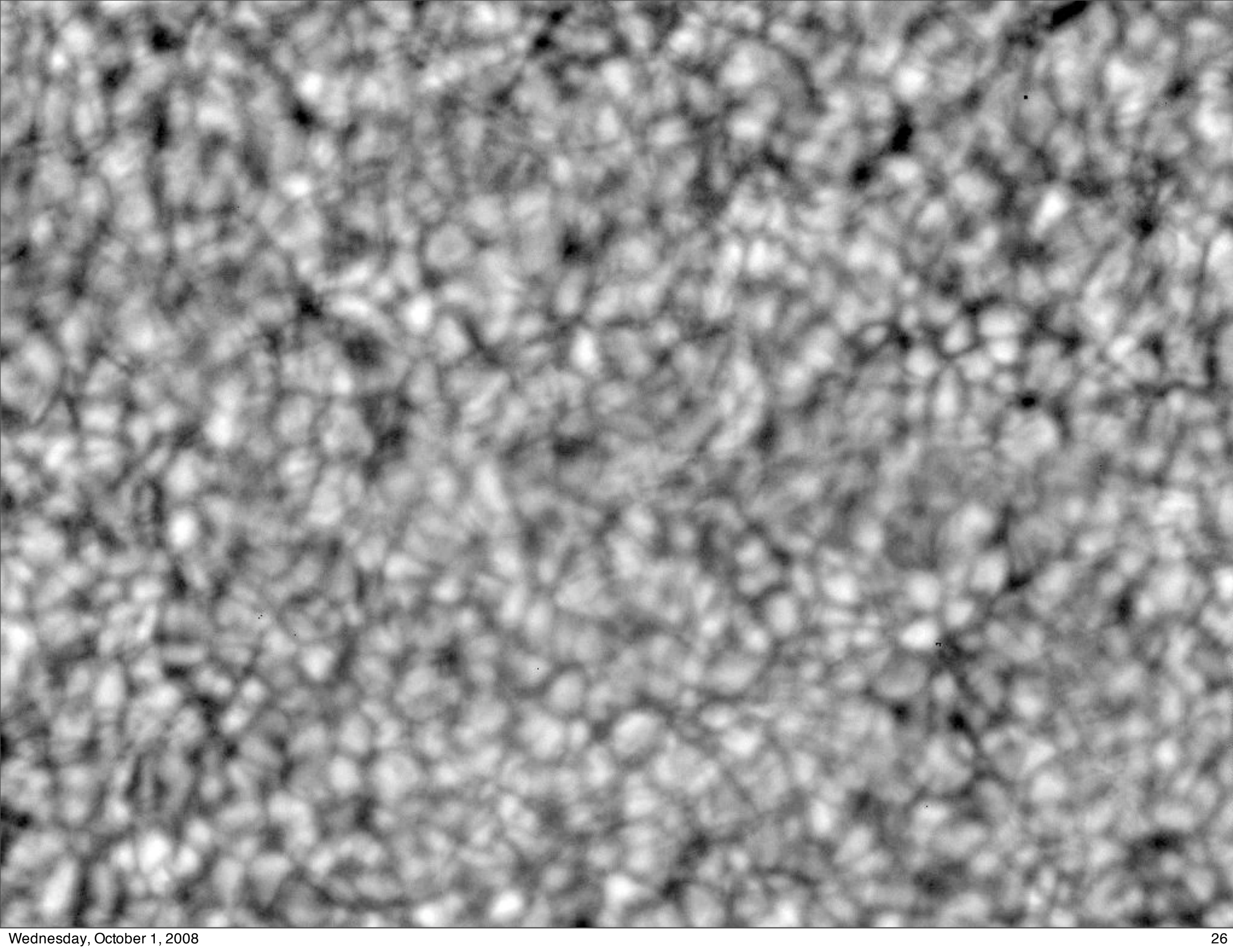
Karhunen-Loeve functions

Karhunen-Loeve functions are similar to Zernikes but with important advantages:

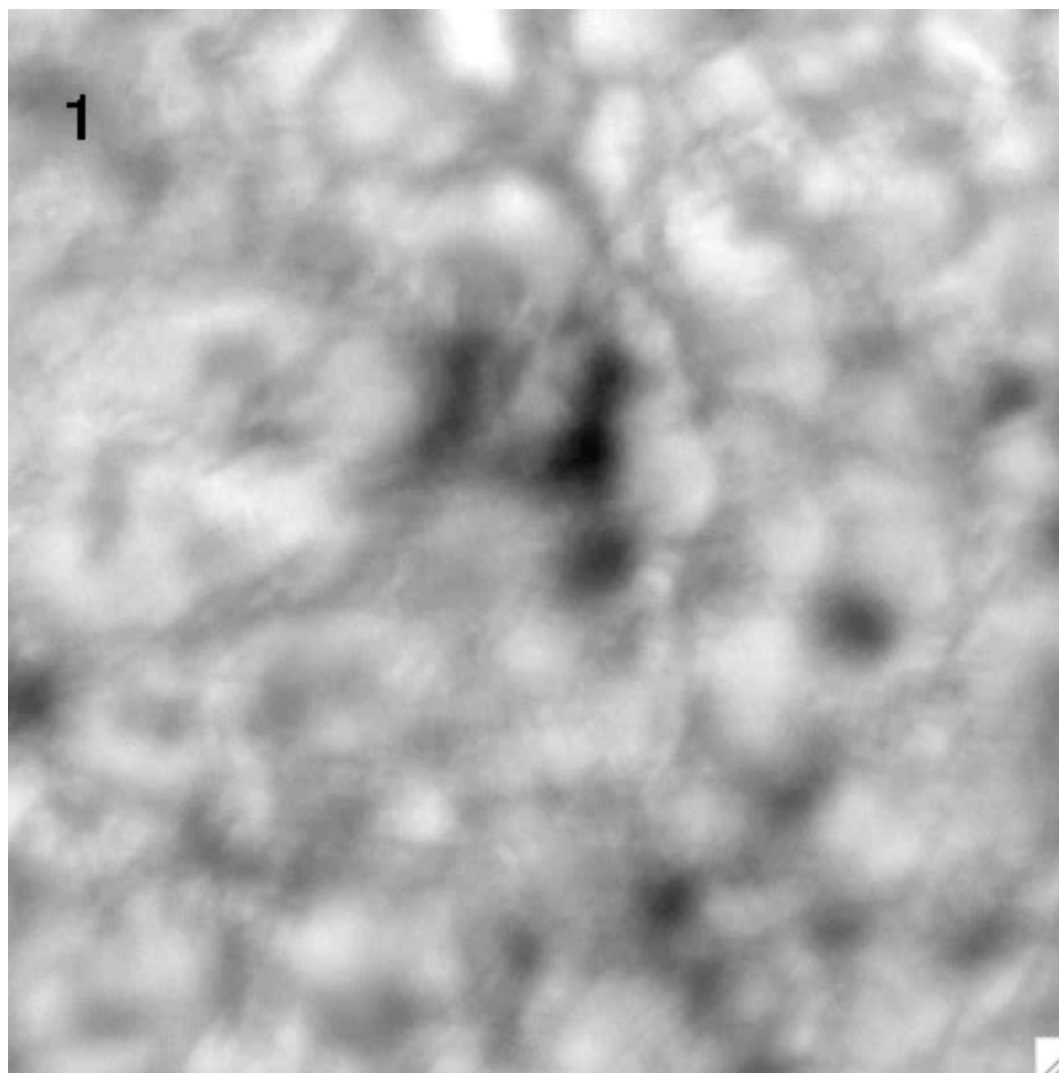
- When expanding atmospheric wavefronts (consistent with Kolmogorov theory) into Karhunen-Loeves (KL's) with coefficients C_n , the coefficients C_n are statistically independent
- KL polynomials are the optimum expansion of atmospheric seeing in the sense that compensating the KL's with the largest amplitudes gives the highest possible reduction of the wavefront RMS from atmospheric seeing.
- High-order KL's have smoother behaviour near the edge of the pupil than Zernikes, giving better match to optical components for Adaptive Optics

Karhunen-Loeve functions





continuum at 436.4 nm



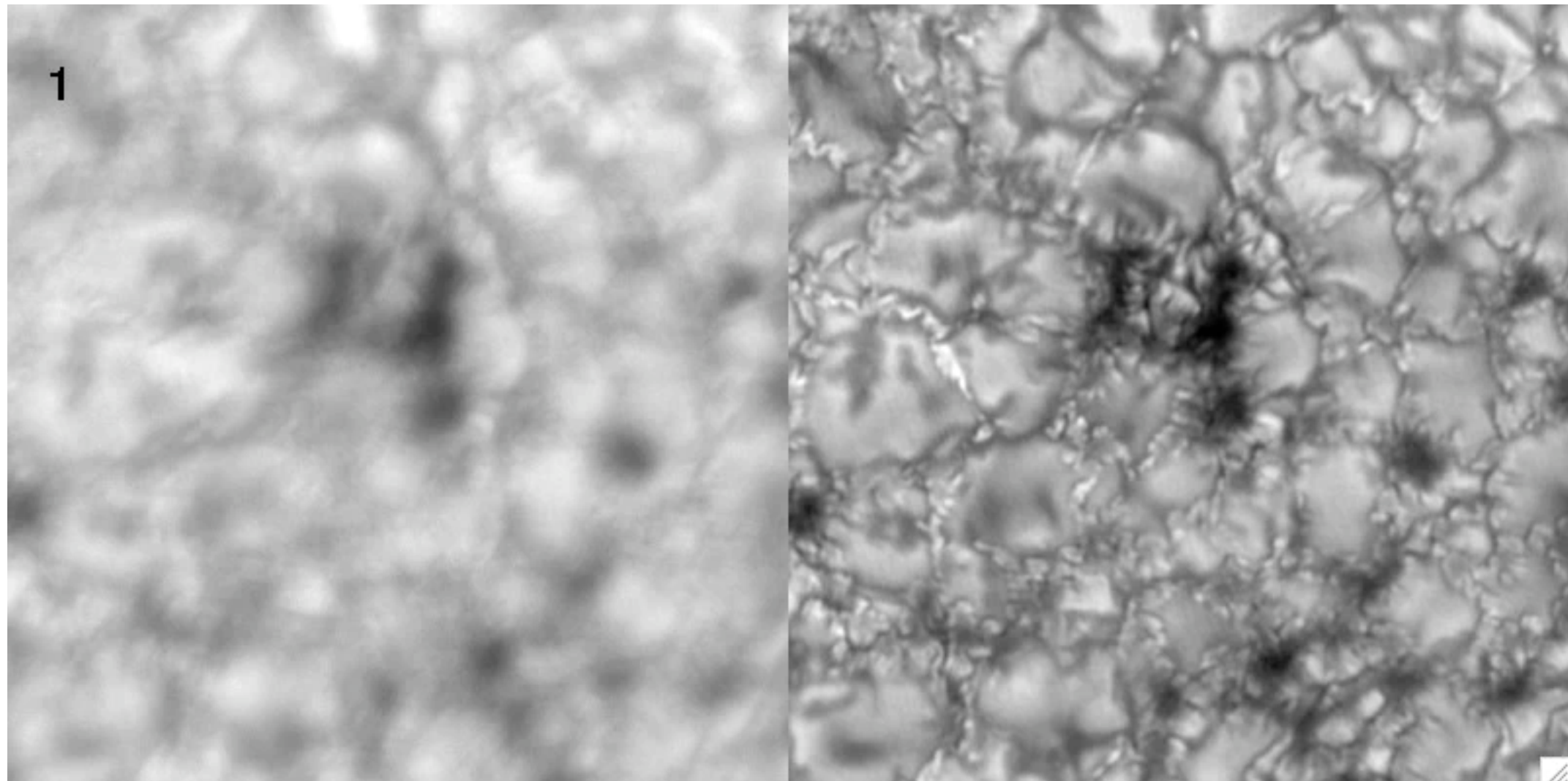
raw images, 2 fps
AO less than 100% lock

Multi-Object Multi-Frame Blind Deconvolution

image processing

(MOMFBD, van Noort et al. 2005, Sol. Ph. 228)

continuum at 436.4 nm

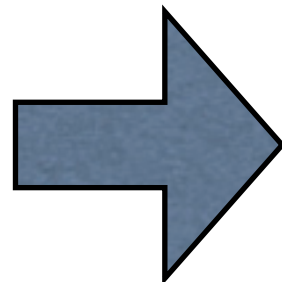


raw images, 2 fps
AO less than 100% lock

MOMFBD restored
10 realizations,
Gcont+pd + Gband+pd

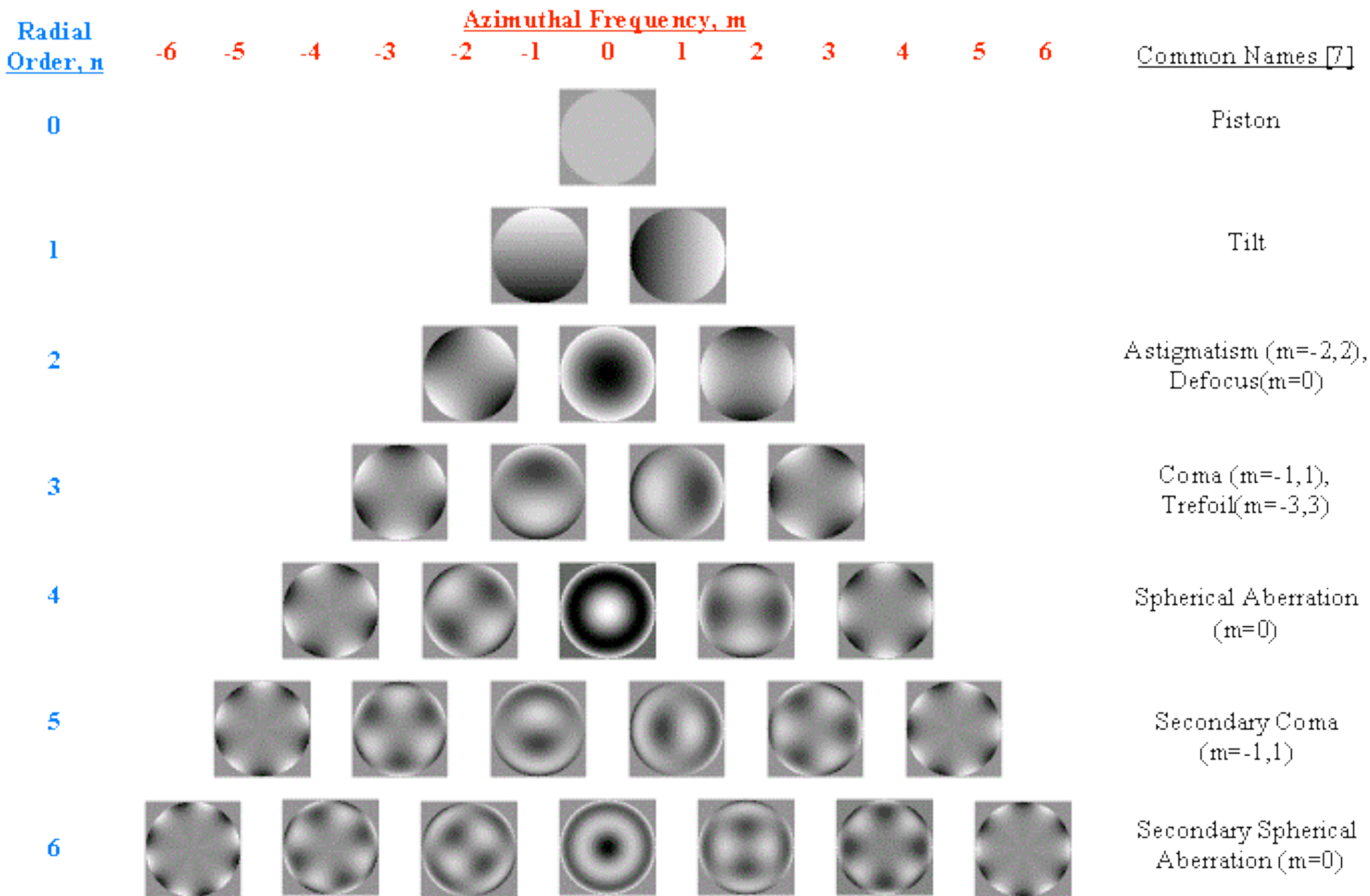
Pupil function
(wavefront aberration)

Fourier Transform (FT)

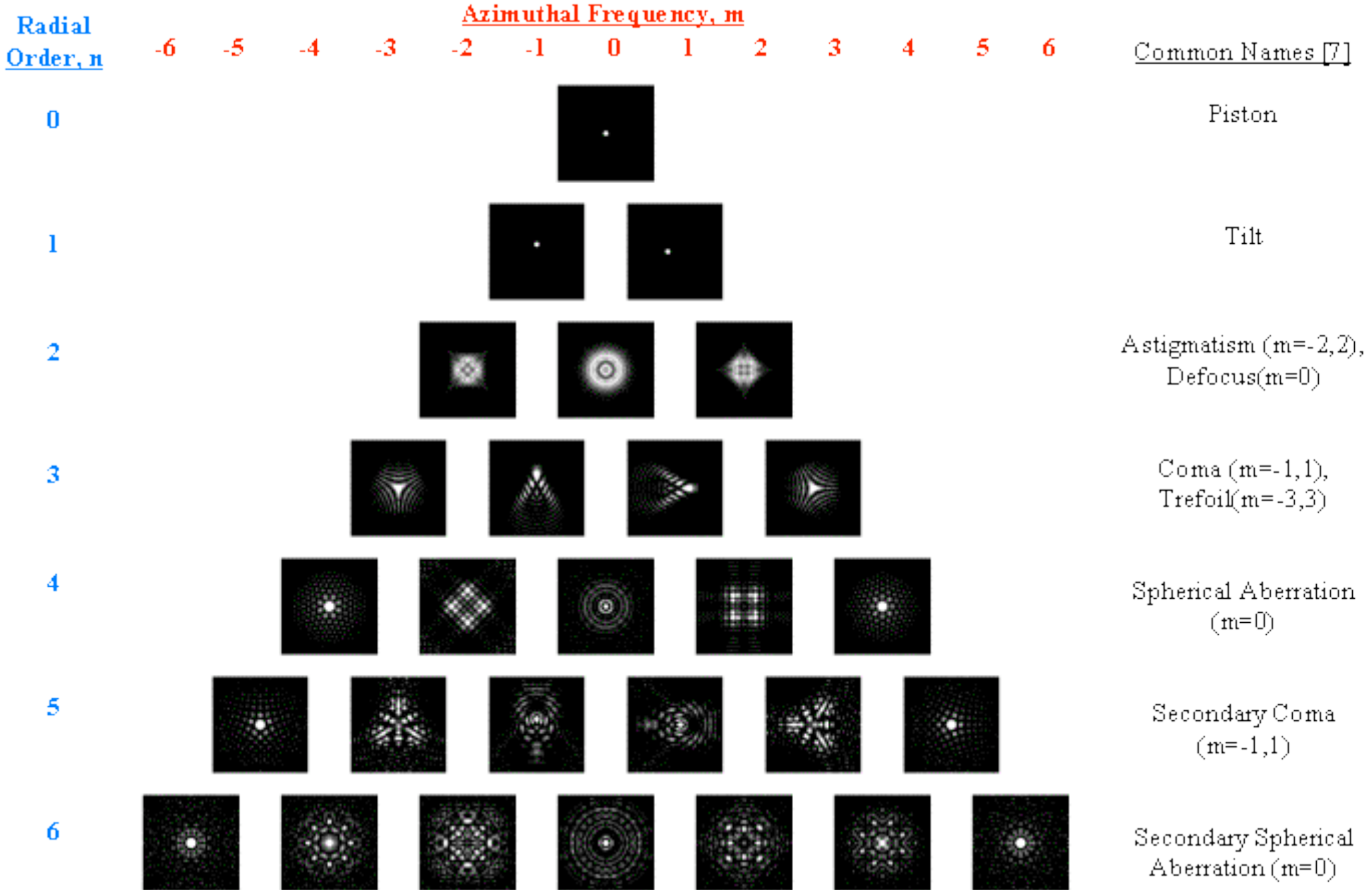


Point Spread Function
(PSF)

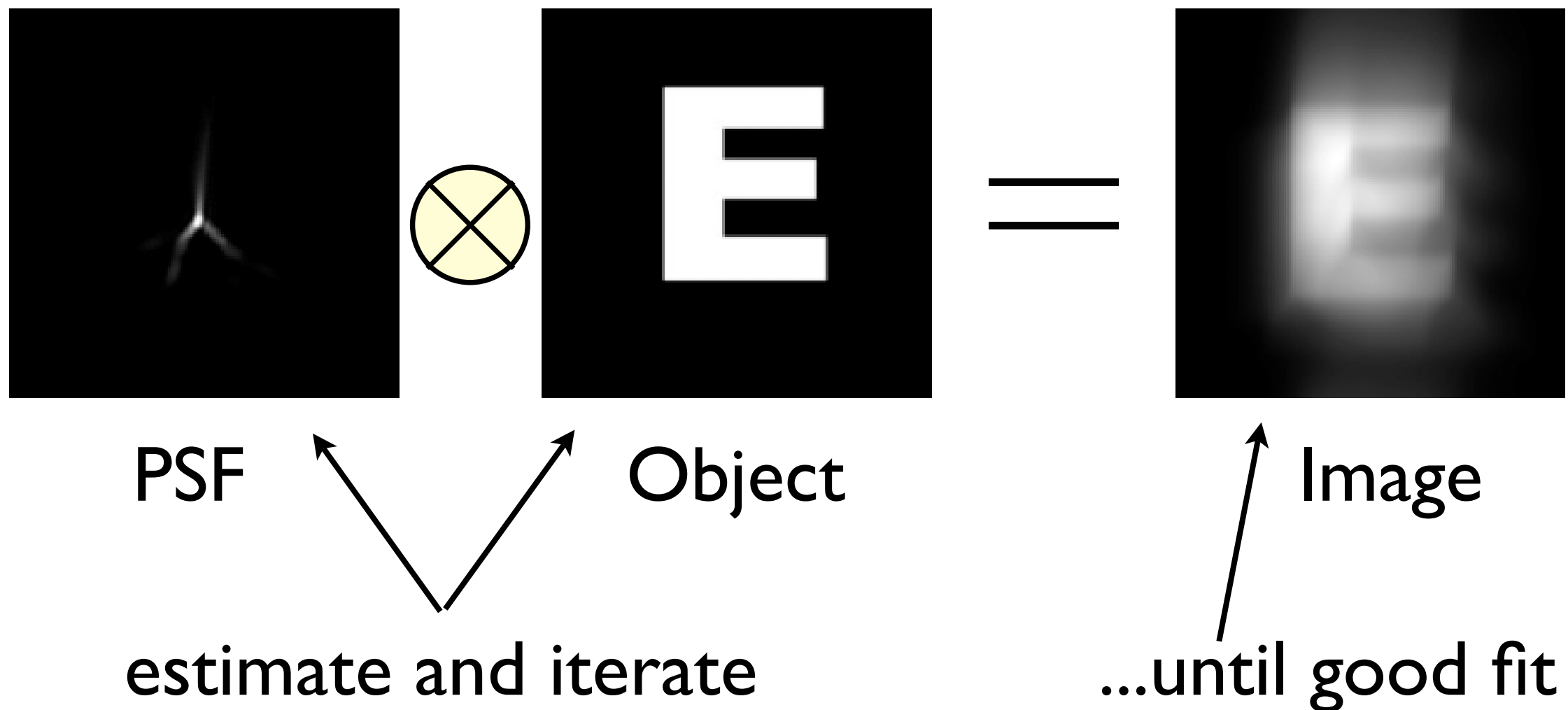
Zernike polynomials up to 6th order



...corresponding PSFs



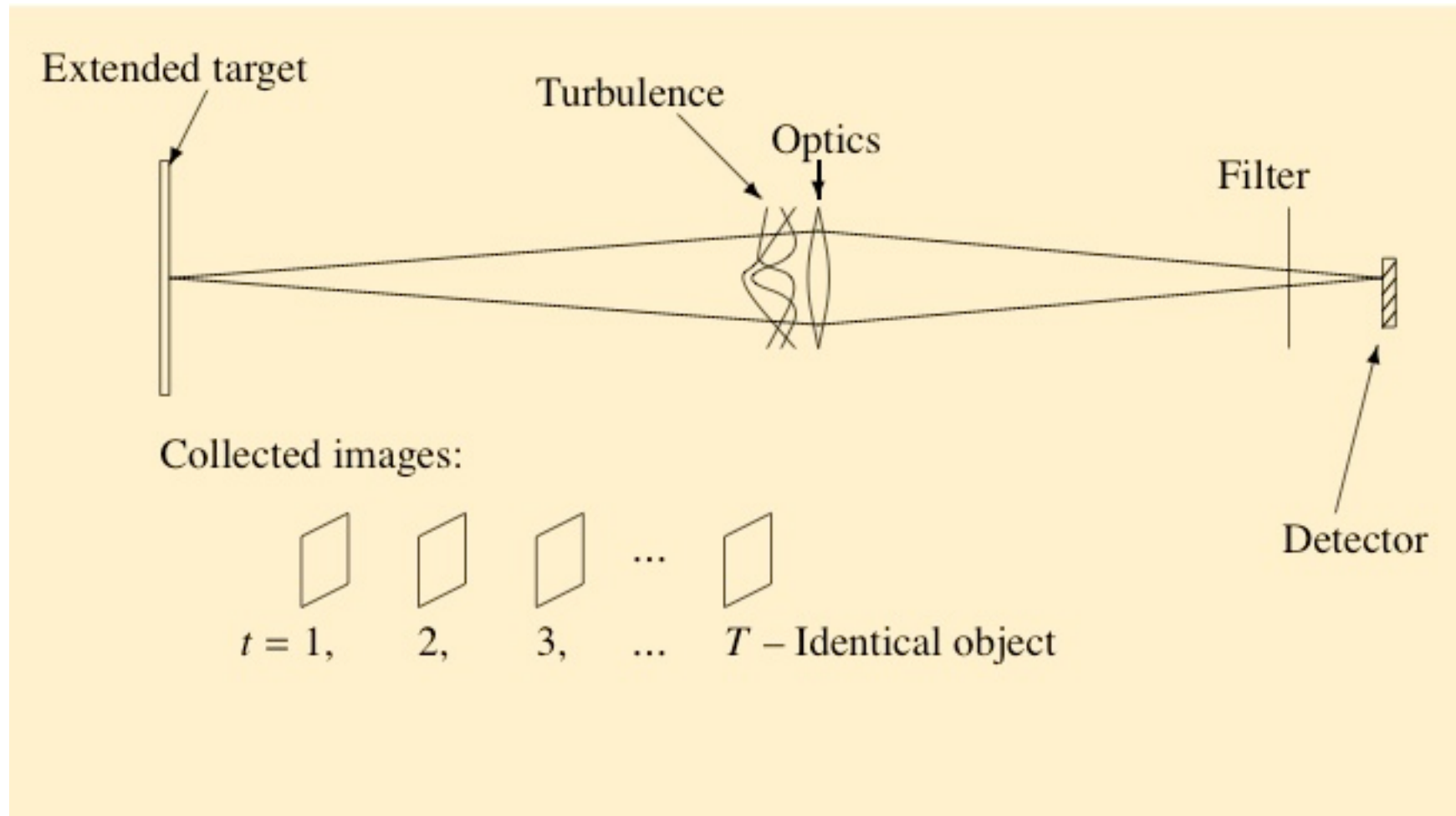
Blind deconvolution



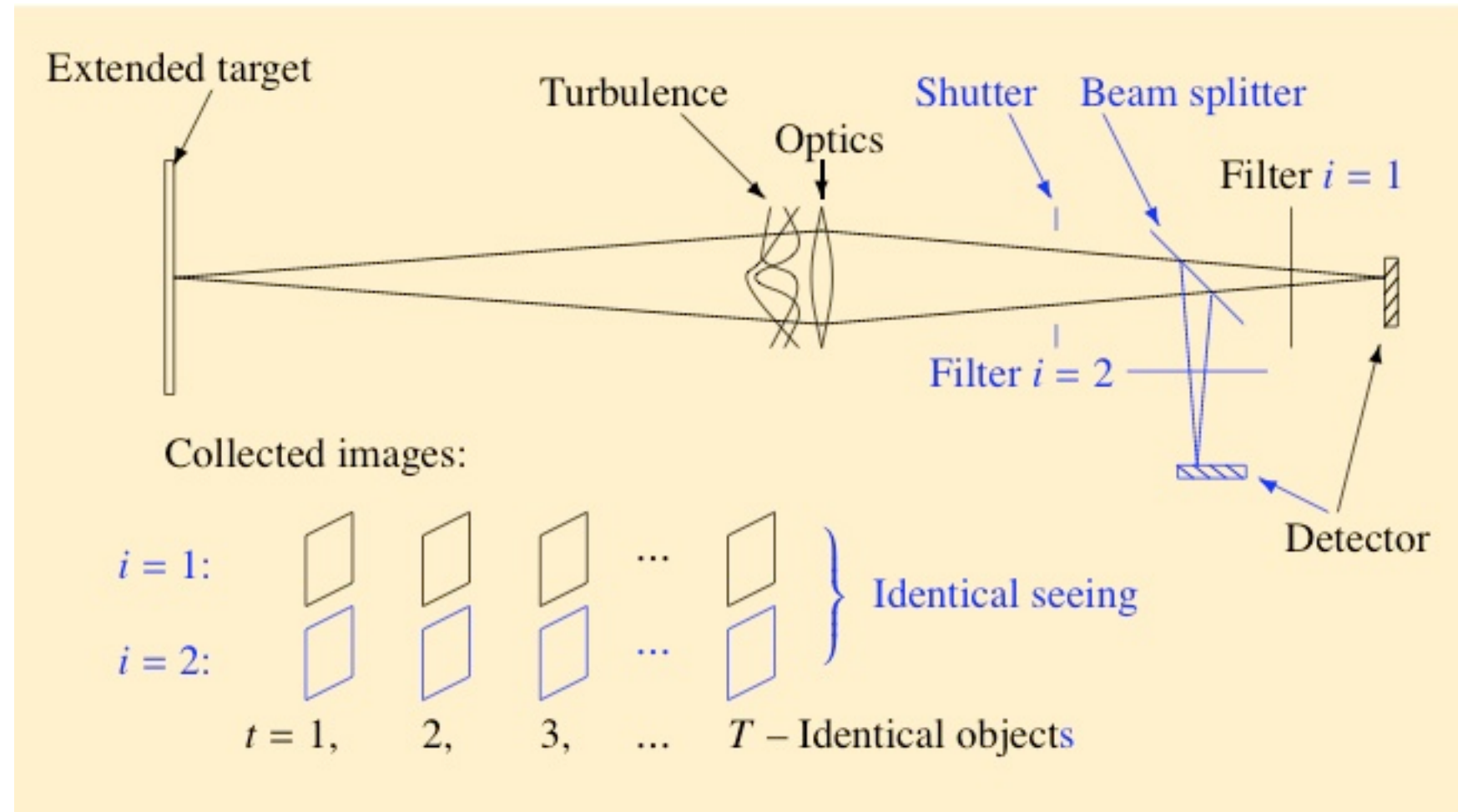
MOMFBD method, key steps

- Image formation model:
 $\text{Image} = \text{PSF} * \text{Object} + \text{noise}$
- parameterize pupil phase: Karhune-Loeve polynomials
- constrain phase parameters using multiple frames, phase diversity, multiple objects
- Fit estimated Object * PSF to observed images by iterative minimization of error metric.

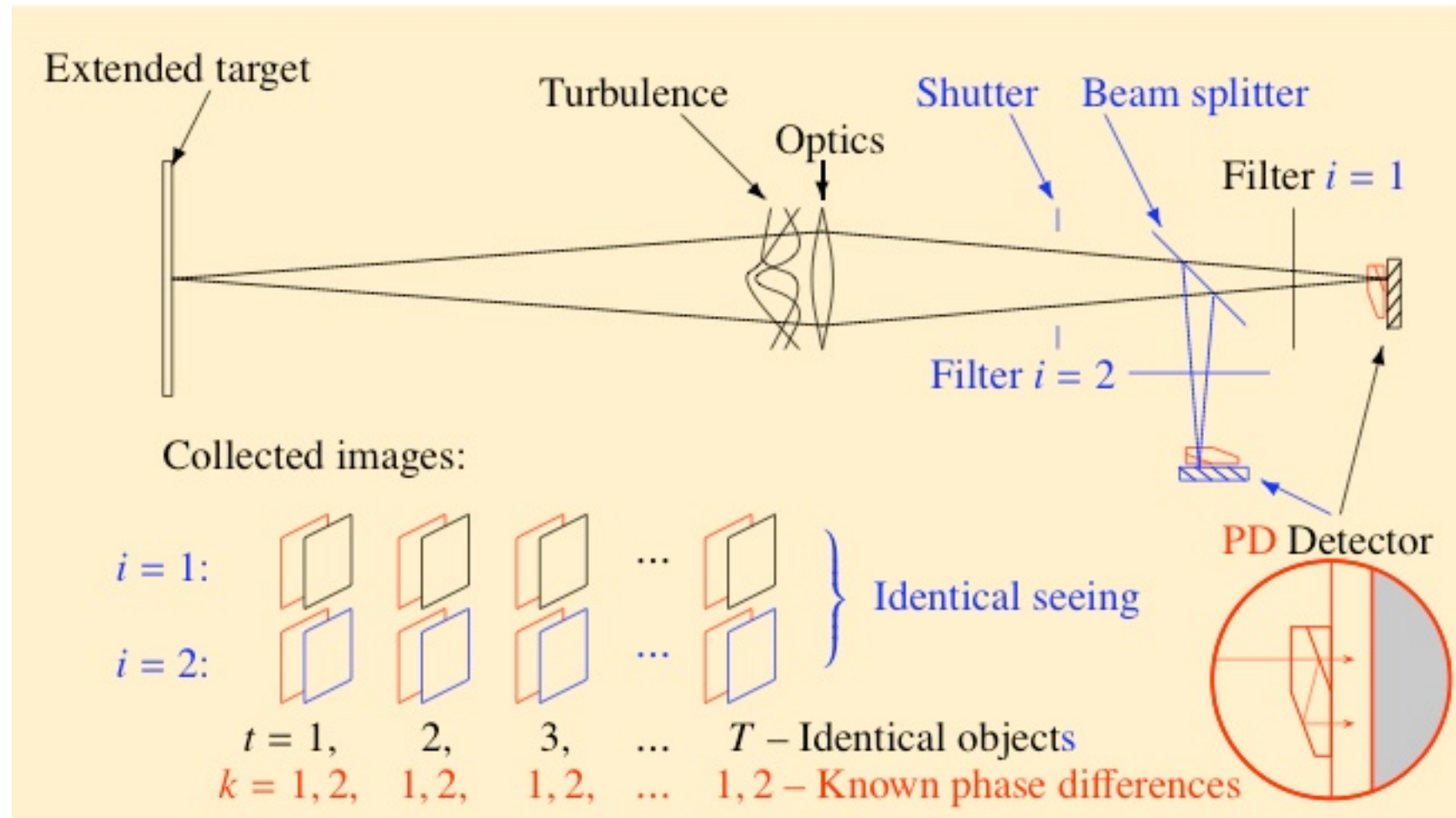
Multi-Frame Blind Deconvolution



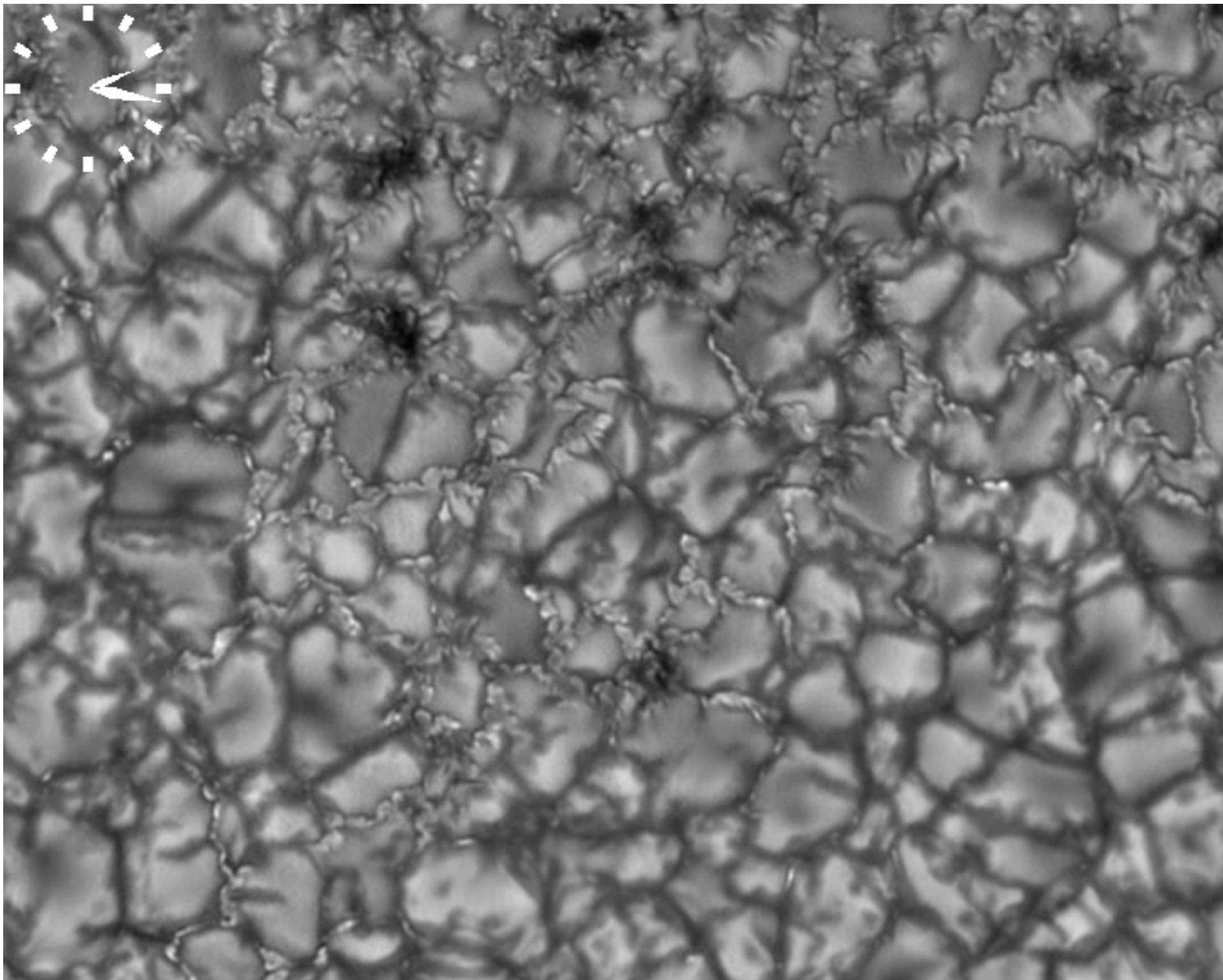
Multi-Object Multi-Frame Blind Deconvolution



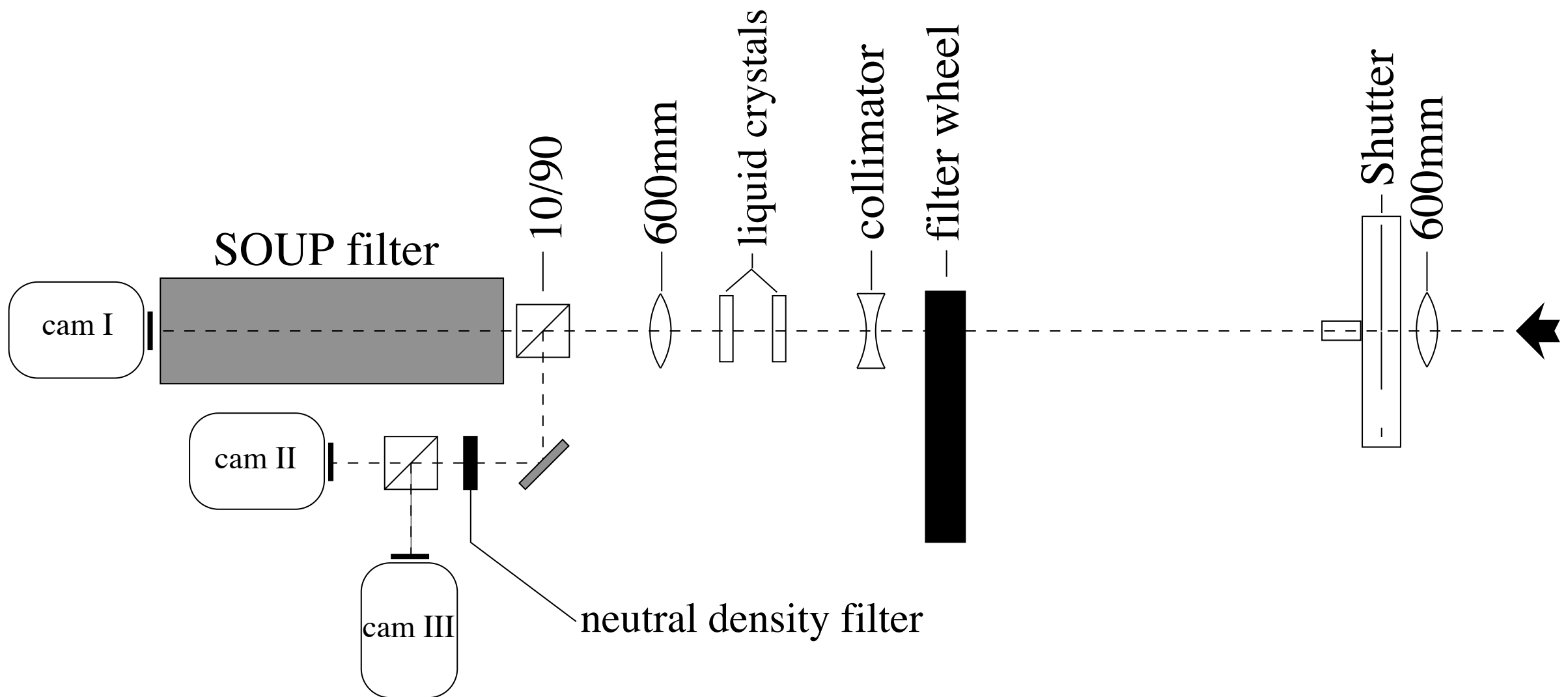
Multi-Object Multi-Frame Blind Deconvolution with phase-diversity



| 3 May 2004: continuum at 4564 Å, 2h

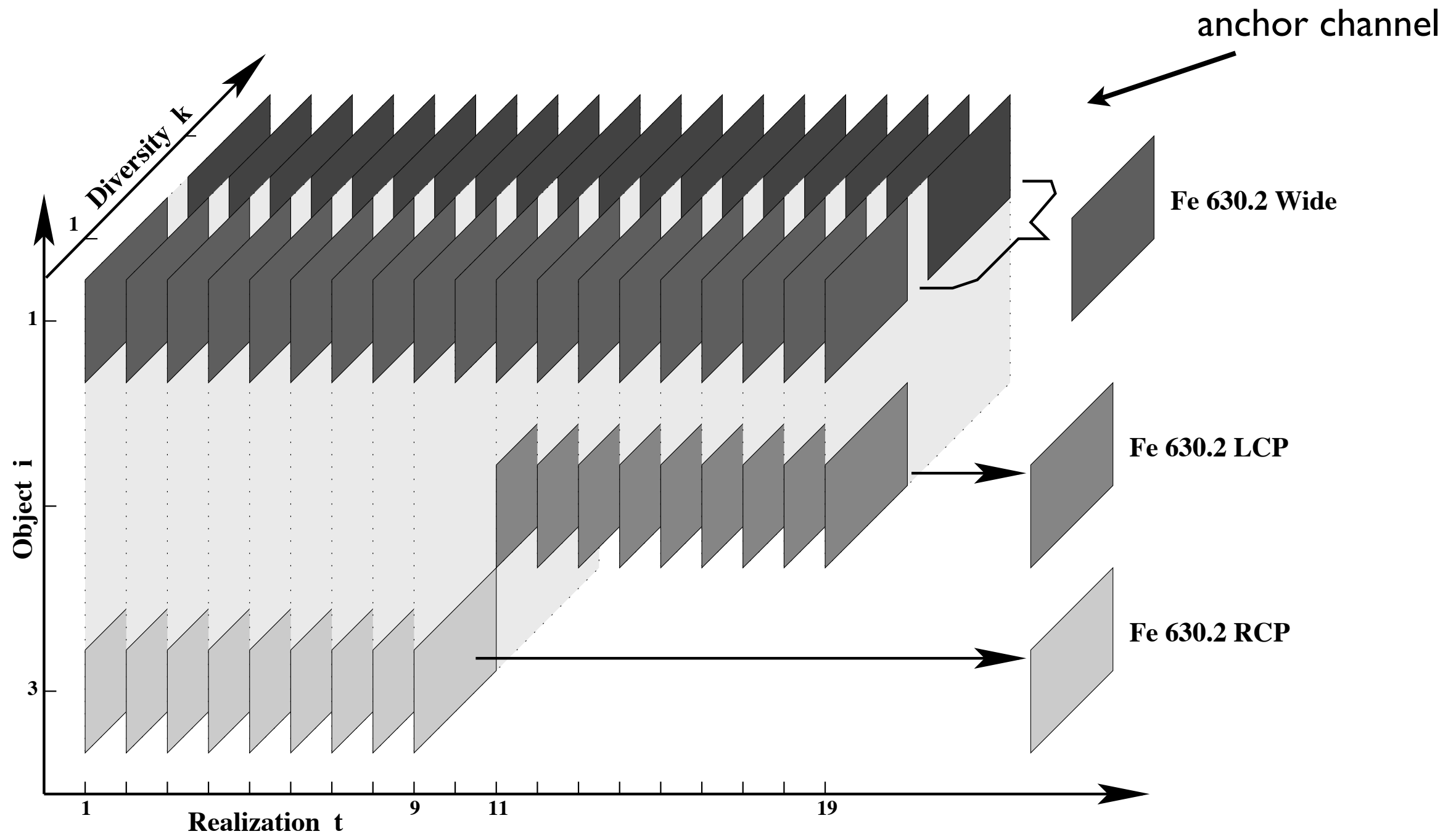


Optical set-up MOMFBD observations



SOUP: Solar Optical Universal Polarimeter
Lyot type narrow band tunable filter

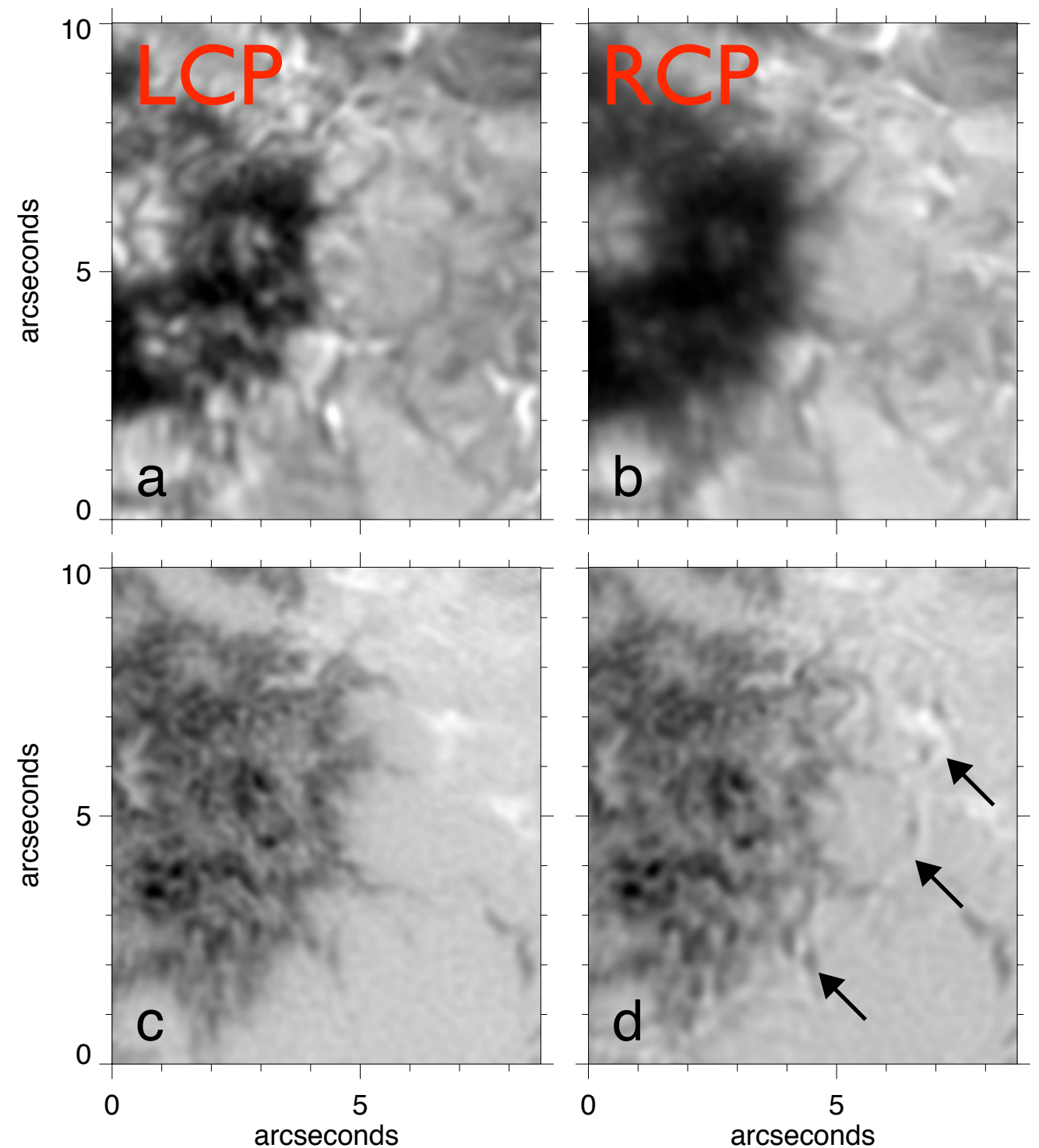
data acquisition model



MOMFBD: perfect alignment

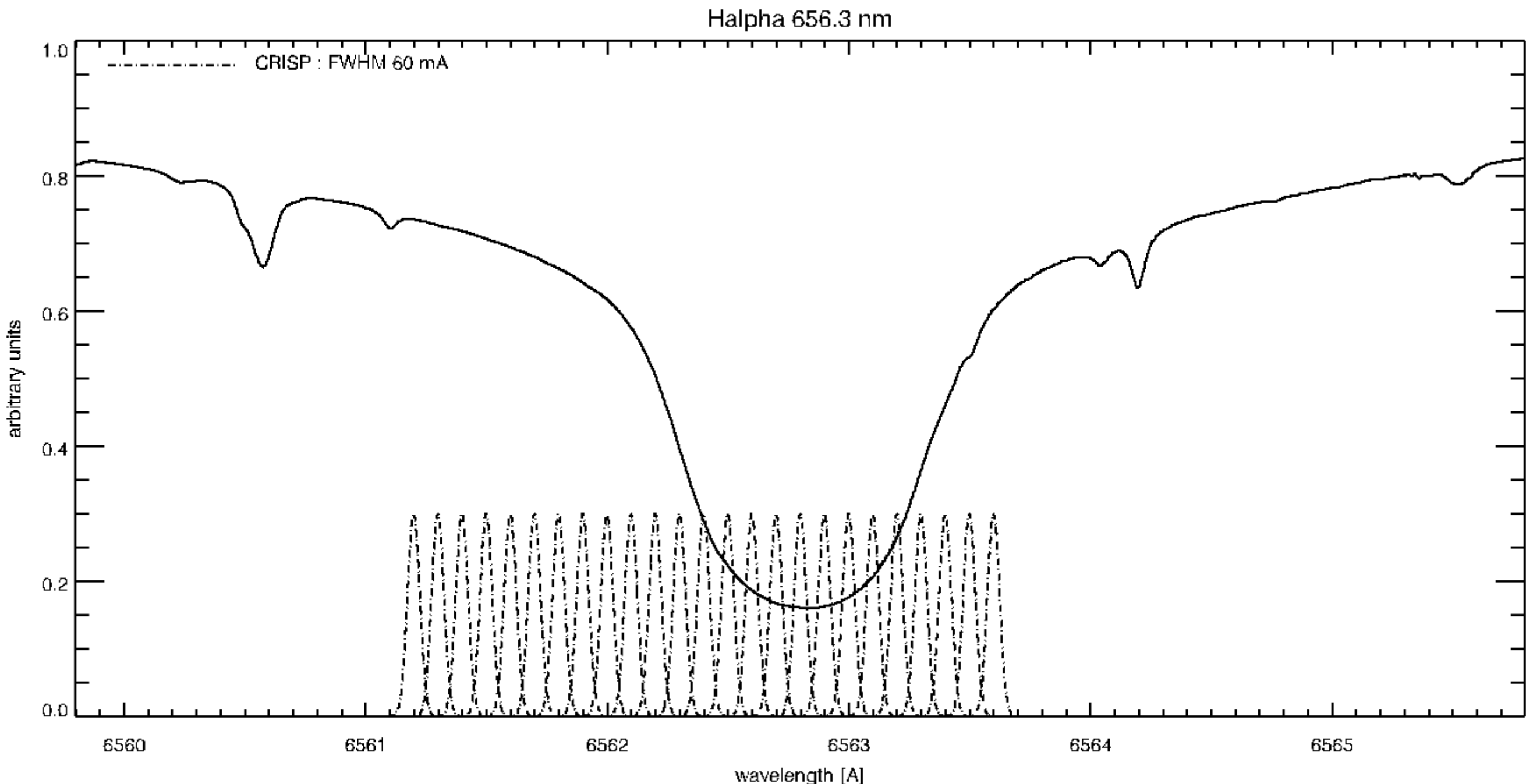
Stokes V magnetogram:
map of circular polarization
(magnetic field along LOS)

$$V = (LCP - RCP) / (LCP + RCP)$$

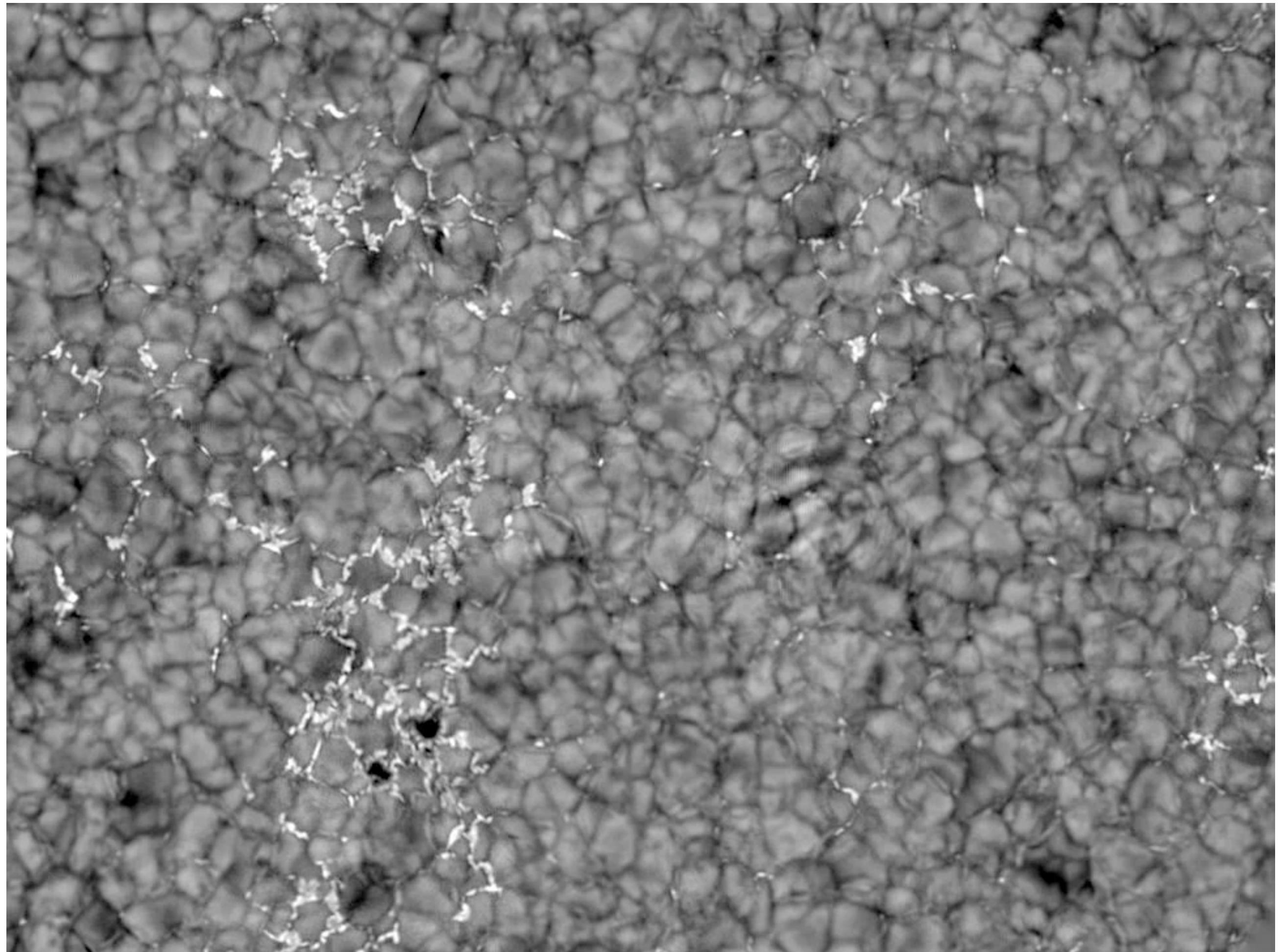


CRISP: CRisp Imaging SpectroPolarimeter

new narrow-band tunable filter at the SST



5 s to record 24 line positions



Swedish 1-meter Solar Telescope

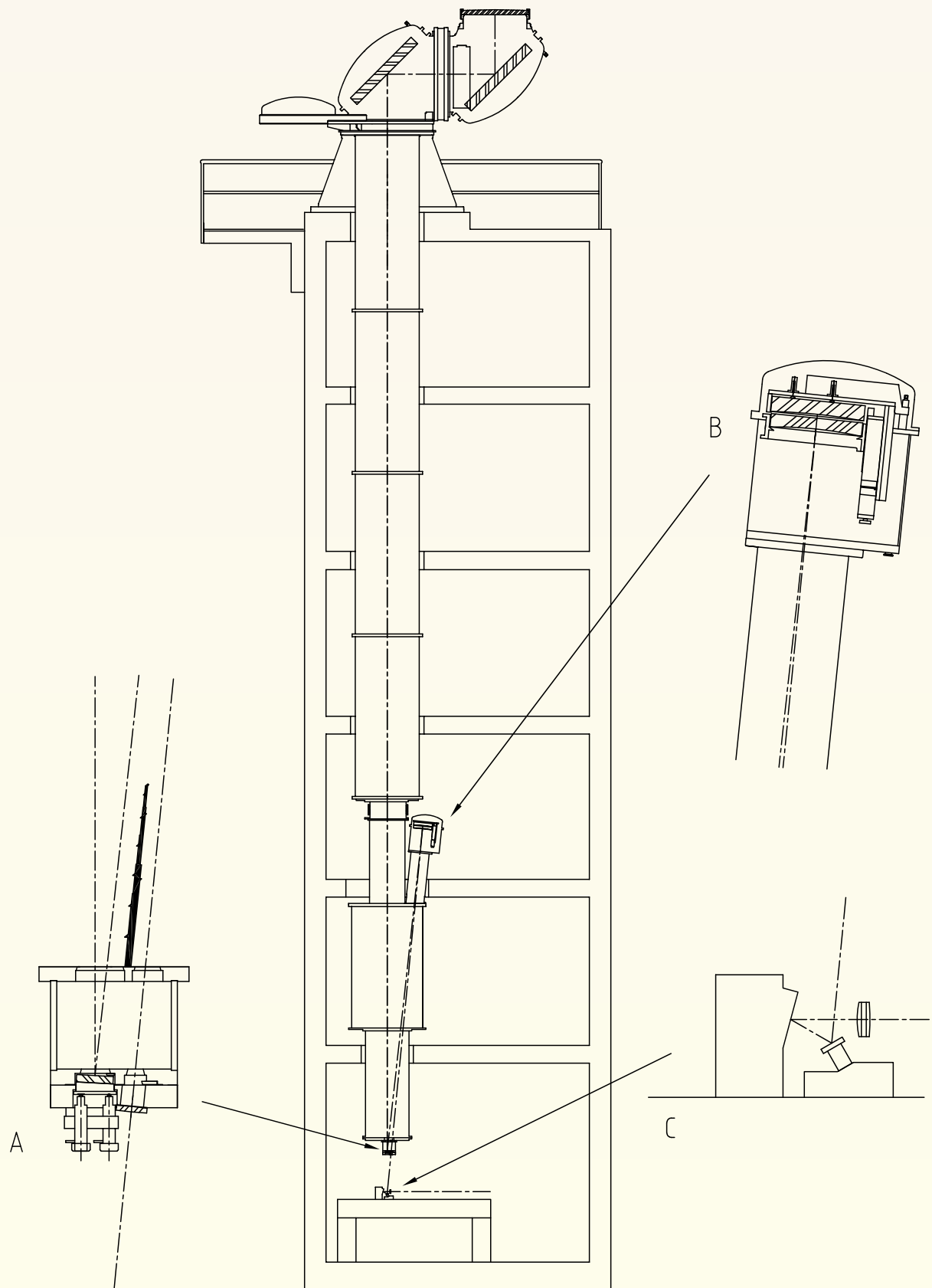
- excellent site
- excellent optics



Observatorio Roque de los Muchachos on La Palma



SST: Swedish 1-m Solar Telescope

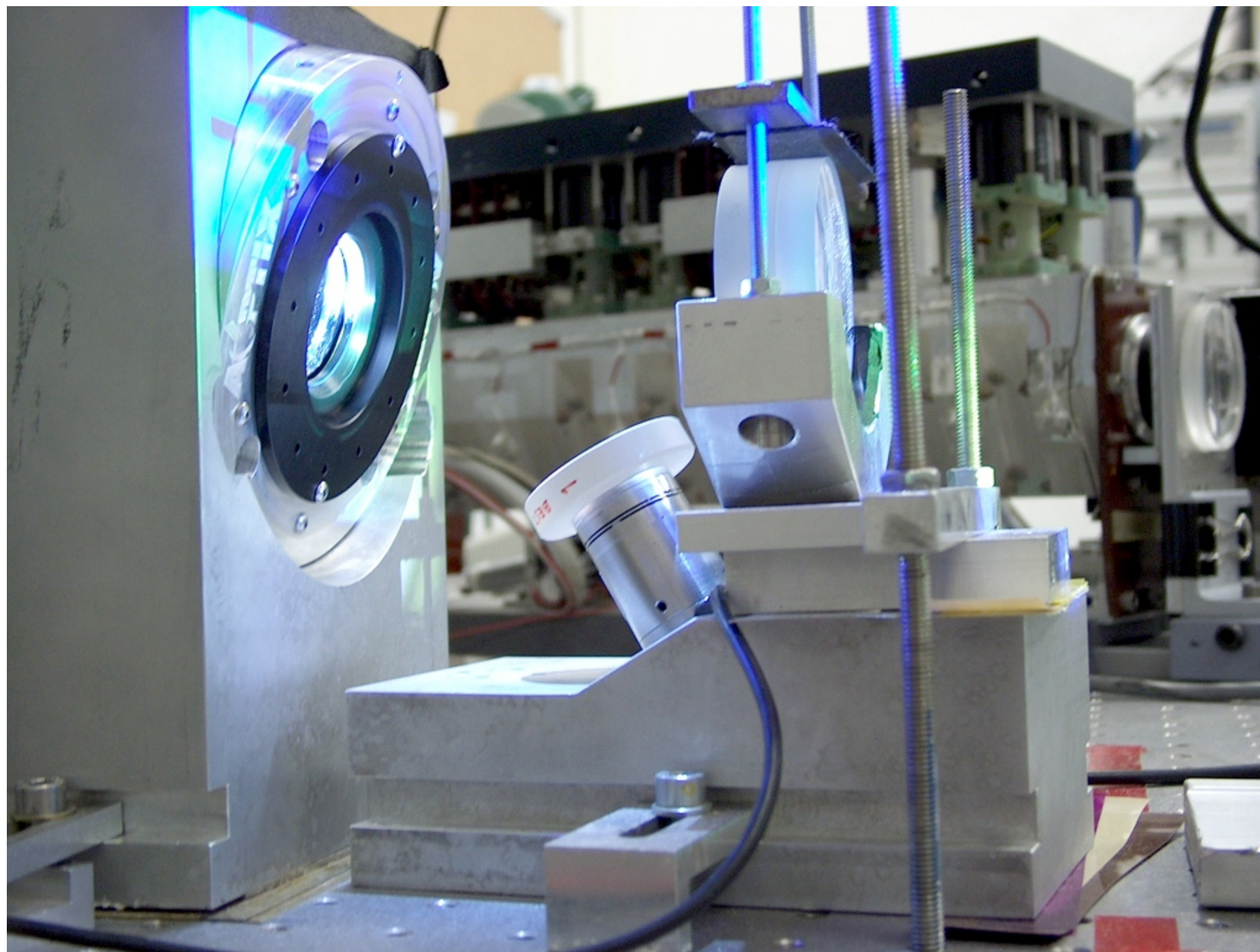


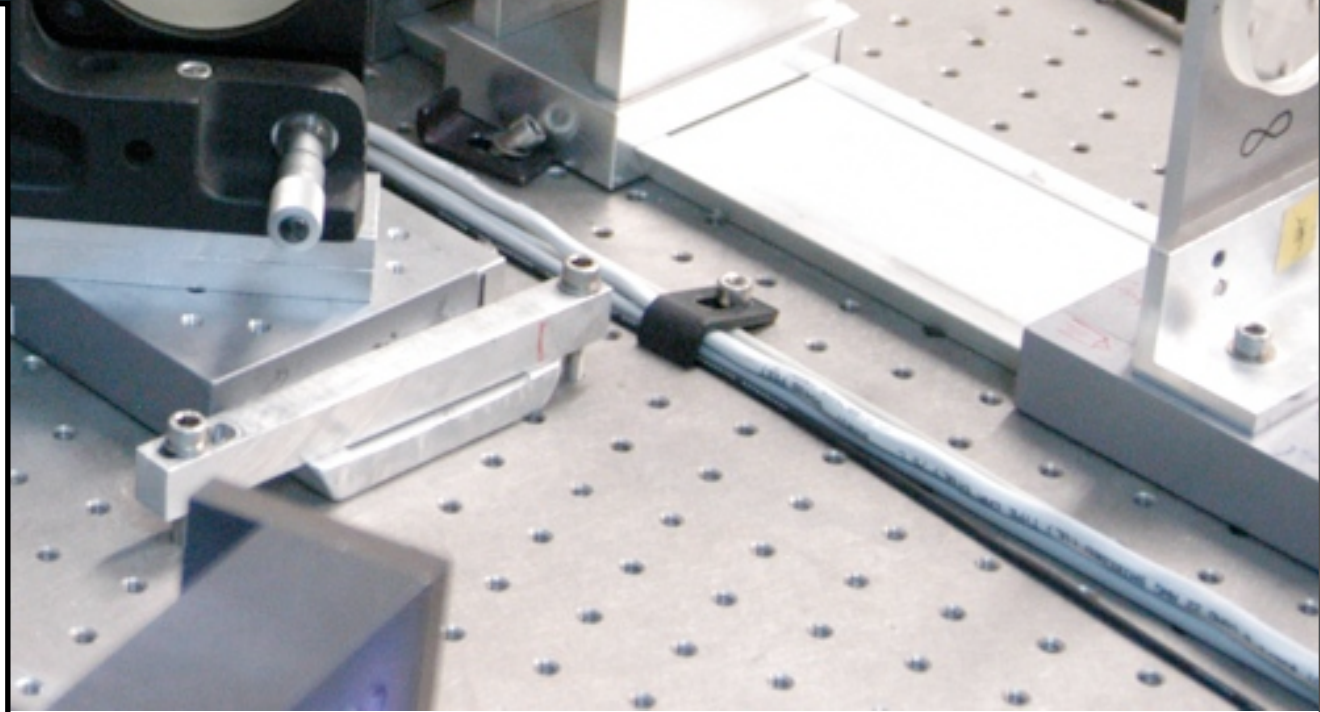
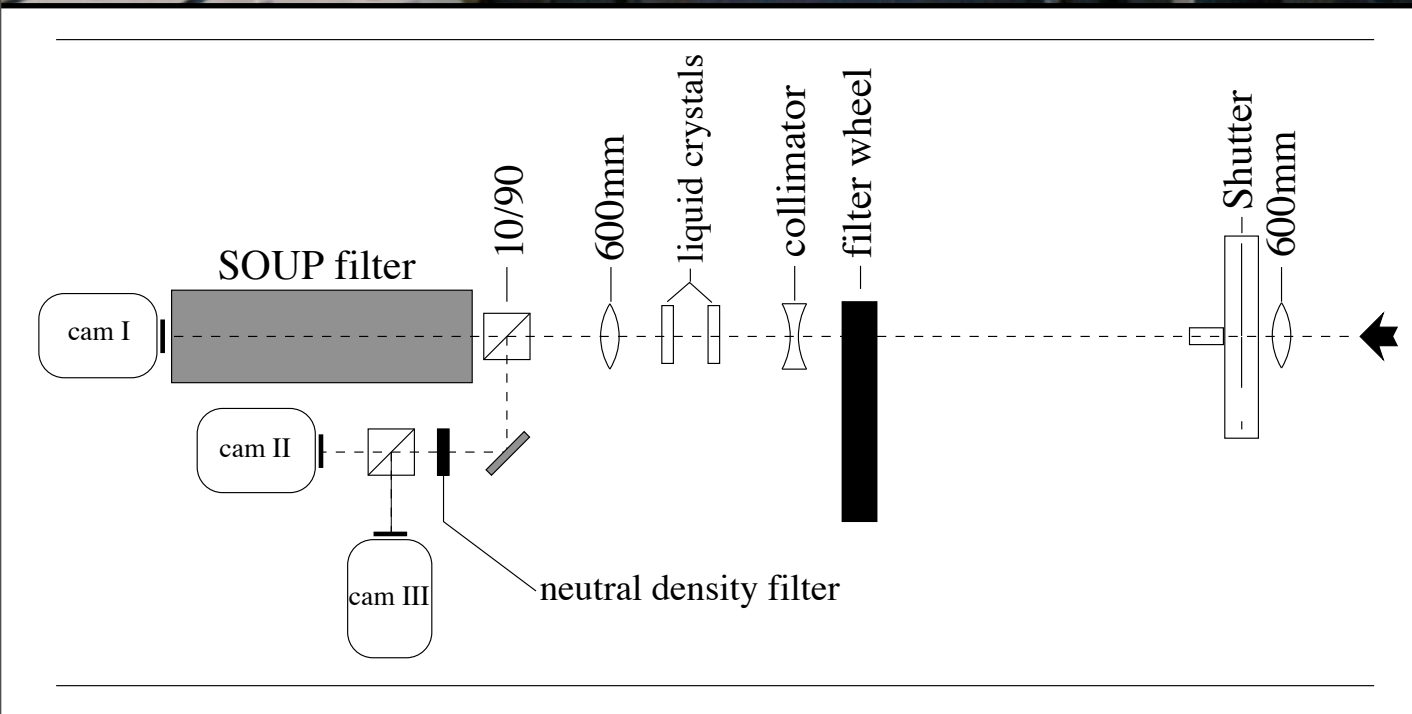
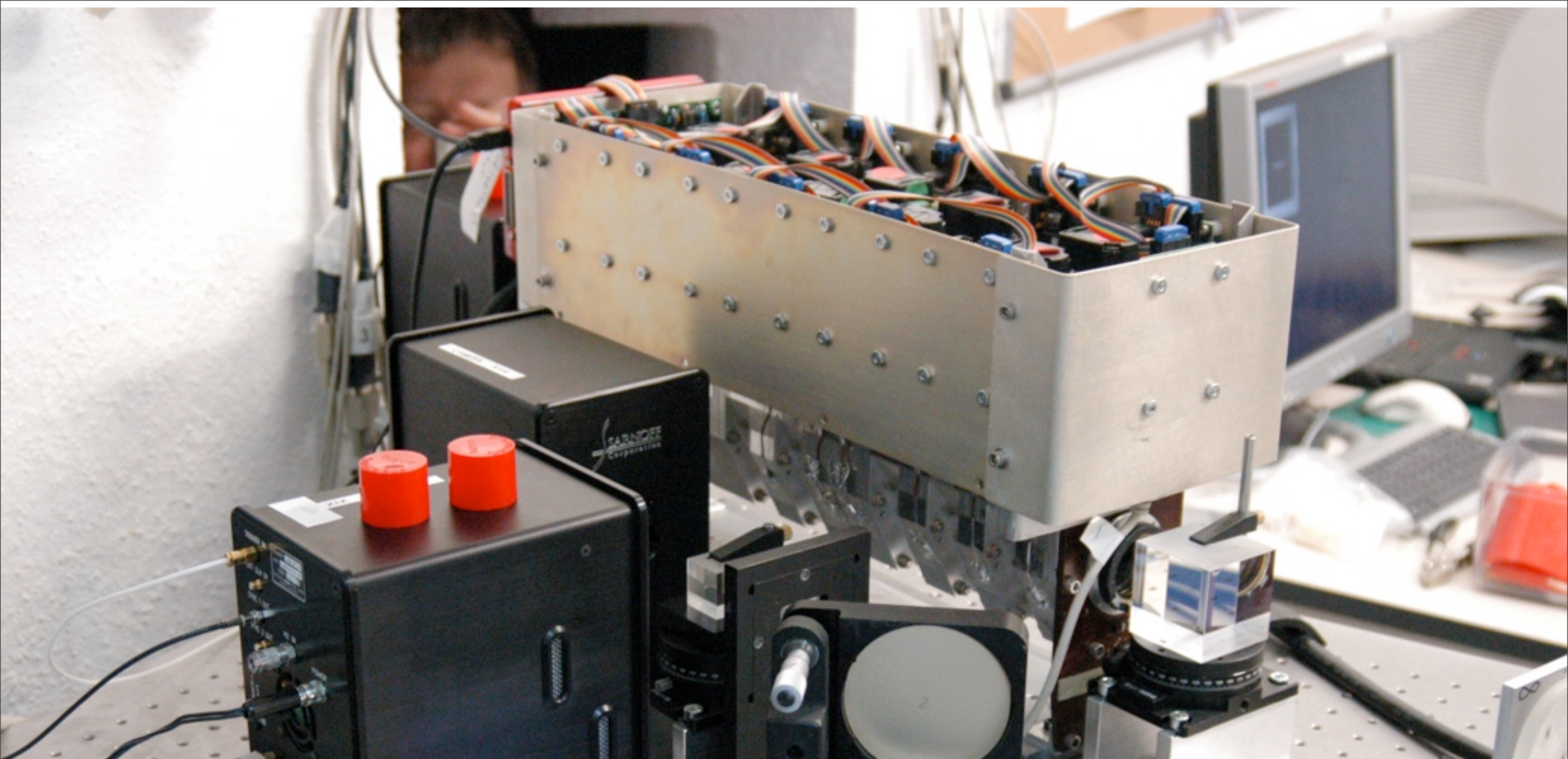
A: field mirror and field lens

B: Schupmann corrector to correct chromatic aberration main objective

C: tip-tilt mirror, deformable mirror and re-imaging lens

Tip-tilt mirror, deformable mirror and re-imaging lens





data rate

- 3 1024x1024 pixel CCD cameras, 37 frames per second → 72 MB/s
- 4 2048x2048 pixel CCD cameras, 8 frames per second → 116 MB/s
- total 678 GB/h
- 10 h observing day, 14 day campaign...

95 TB!

ATABeast, 42 hard disks



Pleiades computing cluster



- linux cluster
- 51 nodes, 204 CPU's
- dedicated to SST data processing
- located in ITA machine room

Halpha 656.3 nm

SST 04-Oct-2005

